Investigation of erosion wear of slurry pump material

A Thesis Report Submitted

in partial fulfillment of the requirements for

the award of degree of

MASTER OF ENGINEERING

IN

PRODUCTION AND INDUSTRIAL ENGINEERING

Submitted by

Naveen Saini

Roll No.: 801082023

Under the Guidance of

Dr. S.K. Mohapatra

Sr. Professor MED & Dean Academic Affair

Thapar University, Patiala

DEPARTMENT OF MECHANICAL ENGINEERING

THAPAR UNIVERSITY

PATIALA-147004, INDIA.

June 2012

DECLARATION

I hereby certify that the work which is being presented in the report entitled, **"Investigation of erosion wear of slurry pump material"**, in partial fulfillment of the requirements for the award of degree of Master of Engineering in Mechanical Engineering with specialization in **PRODUCTION AND INDUSTRIAL ENGINEERING** submitted in **Mechanical Engineering Department** of Thapar University, Patiala, is an authentic record of my own work carried out under the supervision of **Dr. S.K. Mohapatra** and refers other researcher's works which are duly listed in the reference section.

The matter presented in this thesis has not been submitted for the award of any other degree of this or any other university.

Naveen Saini

Date: 19/07/12 **(Naveen Saini)**

Place: Patiala

This is to certify that the above statement made by the candidate is correct and true to the best of my knowledge.

Supervisor:

Dr. S.K. Mohapatra
Dean of Academic Affairs
Thapar University, Patiala

Counter signed by

Dr. Ajay Batish
Professor & head
Mechanical Engineering Department
Thapar University, Patiala

Dr. S.K. Mohapatra
Dean of Academic Affairs
Thapar University, Patiala

ACKNOWLEDGEMENTS

Words are often less to revels one's deep regards. With an understanding that work like this can never be the outcome of a single person, I take this opportunity to express my profound sense of gratitude and respect to all those who helped me through the duration of this work.

This work would not have been possible without the encouragement and able guidance of supervisor Dr. S.K. Mohapatra. Their enthusiasm and optimism made this experience both rewarding and enjoyable. Most of the novel ideas and solutions in this work are the result of our numerous stimulating discussions. Their feedback and editorial comments were also invaluable for the writing of this thesis. I am grateful to Dr. Ajay Batish, Head of Department of Mechanical Engineering Department for providing me the facilities in the Department for the completion of my work.

I take pride of myself being son of ideal parents for their everlasting desire, sacrifice, affectionate blessings, and help, without which it would not have been possible for me to complete my studies.

I would like to thanks Mr. Satish Kumar, Assistant Professor, MED for their novel ideas and solutions in completion of this thesis work.

I am also very grateful to my all friends (Kapil Chawla & Sukhdeep Singh) for accompanying me during the most outstanding year of my life and standing by me in every situation.

I would like to thank to all the faculty members and employees of Mechanical Engineering Department, Thapar Univeristy, Patiala for their everlasting support.

Last but not least, I would like to thank God for all good deeds.

Naveen Saini

(Naveen Saini)

ABSTRACT

Over the last few decades there has been a phenomenal growth in the demand of raw materials. This rise in demand has led to drastic changes in the existing techniques of mining, food processing, power generation and other sectors where transportation of suspended solids play a major role. Due to this change, there has been an increase in requirements in slurry transportation.

Material loss due to erosion wear is a serious problem associated with flow of solid-liquid mixtures. Slurry erosion limits the useful life of equipment and there efficiency. Erosion is therefore a critical parameter for design, selection and operation of the hydraulic transportation system. Engineering interest is to estimate the service life of equipment / components subjected to slurry erosion and to investigate the possibilities of enhancement of their life. As per the application different materials are used.

In the present work evaluation of erosion wear for centrifugal slurry pump is done experimentally as well as numerically. Depending upon applications different materials are selected which are used in centrifugal slurry pumps. The materials selected for present study for centrifugal slurry pump are stainless steel 316 and stainless steel 420. The slurry pot tester is used to evaluate the erosion wear by ash with water solid liquid mixture. Ash required for testing purpose was collected from Guru Govind Singh thermal power plant, Ropar, Punjab. Maximum particle size of solids is 2000μ. Effect of concentration and flow rate of slurry at different speeds is evaluated. . It is experimentally observed that erosion wear is a function of velocity of slurry. As velocity increases erosion wear rate proportionally increses. For numerical simulation ANSYS CFX 13.0 used for evaluation of erosion wear at different concentrations, mass flow rate and speeds.

LIST OF CONTENTS

LIST OF FIGURES

LIST OF TABLES

CHAPTER 1

INTRODUCTION

1.1 PUMP

A pump is a device which converts the mechanical energy into hydraulic energy. The hydraulic energy is in the form of pressure energy. A pump moves liquids from lower pressure to higher pressure. Pump that draws a fluid into itself through a suction port and forces the fluid out through an exhaust port. These applications depend predominantly upon the discharge characteristics of the pump.

Types of Pumps

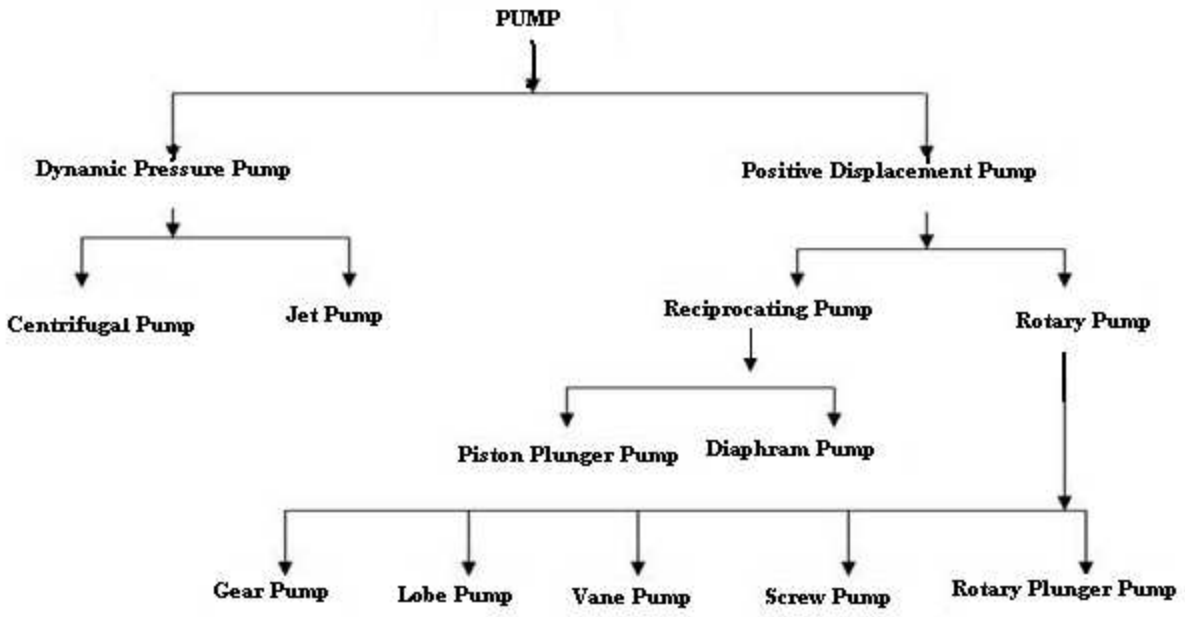

Figure 1.1 Types of pumps

Pump is classified into two categories as shown in figure1.1. A dynamic pump is a kinetic machine in which energy is continuously imparted to the pumped fluid by means of a rotating impeller, propeller, or rotor, in contrast to a positive displacement pump in which a fluid is moved by trapping a fixed amount of fluid and forcing the trapped volume into the pump's discharge. Examples of dynamic pumps include adding kinetic energy to a fluid such as by using a centrifugal pump to increase fluid velocity or pressure. The positive displacement pump operates by alternating of filling a cavity and then displacing a given volume of liquid. The positive displacement pump delivers a constant volume of liquid for each cycle against varying discharge pressure or head.

1.2 CENTRIFUGAL PUMPS

If the mechanical energy is converted into pressure energy by means of centrifugal force acting on the fluid, the hydraulic machine is called centrifugal pump. The flow in a centrifugal pump is in radial outward direction. The centrifugal pump works on the principle of forced vortex flow which means that when certain mass of liquid is rotated by an external torque, which rise in pressure head of rotating liquid takes place. Figure 1.2 shows the diagram of a centrifugal pump.

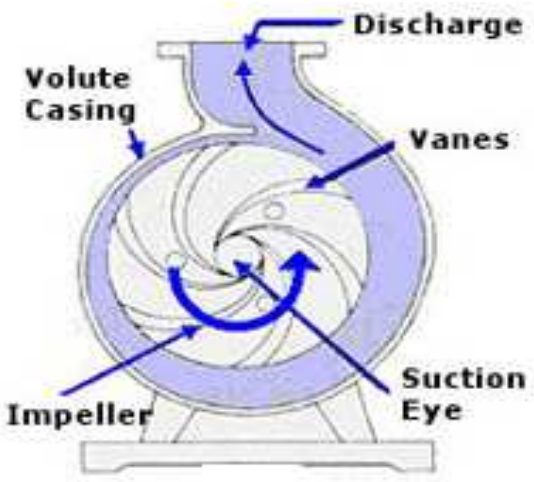

Figure 1.2: schematic diagram of centrifugal pump

1.2.1 Working principle of centrifugal pump

The centrifugal pump works on the principle of forced vortex flow, which means that when a certain mass of liquid is rotated by an external flow, the rise in pressure head of the rotating liquid takes place. The rise in pressure head at any point of the rotating liquid is proportional to the square of tangential velocity of the liquid at that point. Thus at the outlet of the impeller where the radius is more, the rise in pressure head will be more and the liquid will be discharged at the outlet with high pressure head. Due to high-pressure head, the liquid can be lifted to a high level.

1.2.2 Types of centrifugal pumps

Centrifugal pumps can be classified into three general categorized according to the way the impeller imparts energy to the fluid. Each of these categories has a range of specific speeds and appropriate applications.

The three main categories of centrifugal pumps:

1) Radial flow Impeller

2) Mixed Flow Impeller

3) Axial flow Impeller

1.2.2.1. Radial flow impeller

Most centrifugal pumps are of radial flow. Radial flow impellers impart energy primarily by centrifugal force. Water enters the hub and flows radically to the periphery. Flow leaves the impeller at 90 degree angle from the direction it enters the pump.

1.2.2.2. Mixed flow impeller

Mixed flow impellers impart energy partially by centrifugal force and partially as an axial compressor. This type of pump has a single inlet impeller with flow entering axially and discharging in an axial and radial direction. Mixed flow impellers are suitable for pumping untreated waste water. They operate at high speeds than the radial flow impeller pumps; are

usually of lighter construction; and where applicable, cost less than other pumps. Impeller may be either open or enclosed, but enclosed is preferred.

1.2.2.3. Axial flow impeller

Axial flow impeller imparts energy to the water by acting as axial flow compressors. The axial flow pump has a single inlet impeller with flow entering and exiting along the axis of rotation (along the pump drive shaft). These pumps are used in low head, large capacity applications such as water supplies, irrigation, drainage etc.

1.2.3 Main parts of a centrifugal pump

The following are the main parts of centrifugal pumps

1) Impeller

2) Casing

3) Suction pipes with a foot valve and a strainer

4) Delivery pipe

1) Impeller

The rotating part of centrifugal pump is called impeller. It consists of a series of backward curved vanes. The impeller is mounted on a shaft, which is connected to the shaft of an electric motor. An impeller is usually made of iron, steel, aluminium or plastic, which transfers energy from the motor that drives the pump to the fluid being pumped by forcing the fluid outwards from the centre of rotation. Figure 1.6a shows the axial, radial and tangential component of flow.

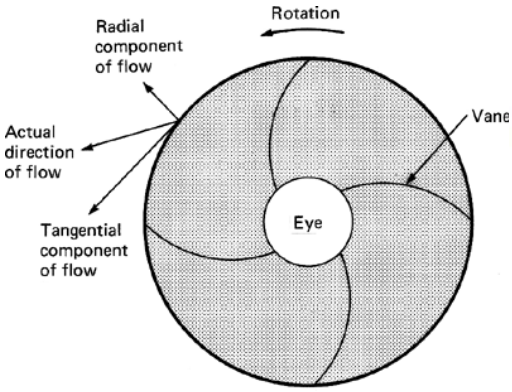

Figure 1.6a Front view of impeller **Figure 1.6b 3D model of impeller**

Components of impeller

a) Blade

Blades are the series of backward or forward curved vanes which transfers the power from shaft to the fluid.

b) Hub and Shroud

The hub is the surface of the machine closest to the axis of rotation. It defines the inner fluid flow surface. The shroud is the surface of the machine farthest from the axis of rotation. It defines the outer fluid flow surface. The hub and shroud can be defined only after the machine data has been defined, although all of these objects can be defined in one step.

c) Leading and trailing edges

The leading edge curve is the most upstream part of the blade. Any change to the leading edge changes the blade surfaces, which changes the periodic surfaces as well as the hub and shroud surfaces. The trailing edge curve is the most downstream part of the blade.

Impellers are also classified as to whether they are:

a) Open impellers:

Most totally open impellers are found on axial flow pumps. This type of impeller would be used in a somewhat conventional appearing pump to perform a chopping,

Figure 1.7 Open Impeller

Grinding action on the liquid. The totally open axial flow impeller moves a lot of volume flow, but not a lot of head or pressure. With its open tolerances for moving and grinding solids, they are generally not high efficiency devices.

b) Semi-open impeller

Figure 1.8 Semi-Open Impeller

A semi-open impeller has exposed blades, but with a support plate or shroud on one side. These types of impeller are generally used for liquids with a small percentage of solid particles from the bottom of a tank or river, or crystals mixed with the liquid. The efficiency of these impellers is governed by the limited free space or tolerance between the front leading edge of the blades and the internal pump housing wall.

c) Enclosed impeller

Totally enclosed impellers are designed with the blades between two support shrouds or plates. These impellers are generally used clean liquids because tolerances are tight at the eye and the housing, and there is no room for suspended solids, crystals or sediment, Figure1.9. Shows a type of enclosed impeller

Figure 1.9Enclosed Impeller

Cavitation damage, play in the bearings, bent shafts and unbalanced rotary assemblies, and any hydraulic side loading on the shaft and impeller assembly.

2) Casing

Casing of a pump is an airtight passage surrounding the impeller and is designed in such a way that the kinetic energy of the water discharged at outlet of the impeller is converted into the pressure energy before the water leaves the casing and enters the delivery pipe.

Types of casing:

a) Volute casing

Volute casing is of spiral type in which area of flow increase gradually. The increase in the area of flow decreases the velocity of flow. The decrease in velocity increases the pressure of the water flowing through the casing. In case of volute casing the efficiency of the pump increase slightly as a large amount of energy is lost due to formation of eddies in this type of casing.

b) Vortex casing

If a circular chamber is introduced between the casing and the impeller, the casing is known as vortex casing. By introducing the circular chamber, the loss of energy due to formation of eddies is reduced considerably. Thus, the efficiency of the pump is more than the pump with volute casing.

c) Casing with guide blades

In this type of casing, the impeller is surrounded by series of guide blades mounted on a ring, which is known as diffuser. The guide vanes are designed in such a way that water from the impeller enters the guide vanes without stock. Also the area of guide vanes increase, thus reducing the velocity of flow through guide vanes and consequently increasing the pressure of water. The water from the guide vanes then passes through the surrounding casing, which is concentric with the impeller.

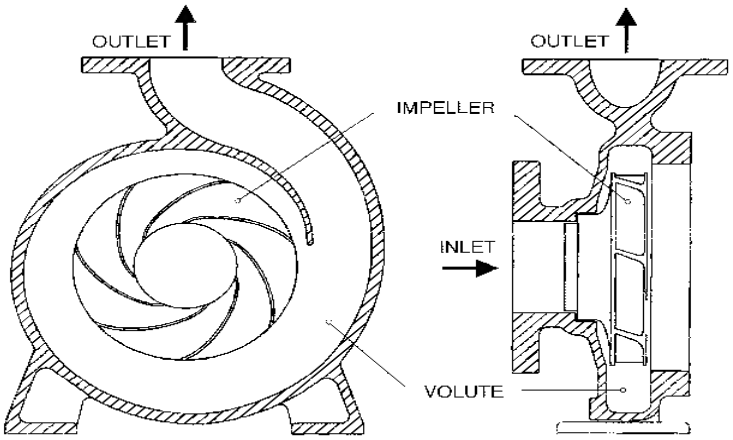

Figure 1.10 Sectional view of centrifugal pump

3) Suction pipe with a foot valve and a strainer

A pipe whose one end is connected to the inlet of the pump and the other end dips into water in a sump is known as a suction pipe. A foot valve, which is non-return valve or one-way type of valve, is fitted at the lower end of suction pipe. The foot valve opens only in the upward direction. A strainer is also fitted at the lower end of suction pipe

4) Delivery pipe

A pipe whose one end is connected to the outlet of the pump and the other delivers the water at the required height is known as delivery pipe. A valve is provided on the delivery pipe to regulate the supply of water. The valve is provided close to the outlet of the pump

1.3 WEAR

Wear is defined as progressive volume loss of material from a solid surface due to corrosion, abrasion and erosion.

Erosive wear

Erosive wear is the dominant process and can be defined as the removal of material from a solid surface due to mechanical interaction between the surface and the impinging particles in a liquid stream. Erosion involves the transfer of kinetic energy to the surface. This means that in erosion material removal is a function of particle velocity squared to higher power. Erosive wear depends on the predominant impact angle of particle impingement with the material surface. Impact angle will vary from 0 to 90 degrees and depend on both fluid particle and particle- particle interaction. This type of wear can be found on impellers and volute casing in slurry pumps, angled pipe bends, turbines, pipes and pipe fitting, nozzles, burners etc. The material loss due to erosion increases with the increase in kinetic energy of the particles impacting at the target surface.

Erosion wear is an important factor in the design and operation of the equipment handling slurries.The volume loss due to erosion is a troublesome problem foe slurry transportation systems e.g. mineral transport systems, ash disposal systems. The erosion wear due to the air borne particles in some devices such as jet planes and turbines is also significant due to very high impact velocity. It is thus a challenging task to control the erosion wear in many engineering applications. The material removal due to erosion is caused by two dominant mechanisms namely brittle fractures and platelet deformations.

In brittle type material, the solid particles impacting on the target surface forms cracks in longitudinal and lateral directions. These cracks propagate due to impact of succeeding particles and broken materials pieces will be carried out by flowing fluid. The material removal rate due to brittle fracture increases with increase in normal component if the particle velocity and thus the brittle type material show maximum wear near normal impact angles.

In Platelet mechanism, the impact of solid particles deforms the target surface to forms hills and valleys. The repeated impacts of particles remove the material and forms crater at the surface. This mechanism along with micro-cutting and chipping dominates in ductile type materials, which show the maximum wear in the impact angle range of 20-40 degree. Apart from the target surface characteristics like brittle or ductile type, many other parameters such as solid particles, carrier fluid, flow conditions etc. affect the erosion wear. It is, therefore, difficult to estimate wear for a given operating conditions.

1.4 TRANSPORTATION OF SLURRY THROUGH PUMP

Slurry is a mixture of solids and liquids. The most commonly used liquid is water. Over the last few decades there has been a phenomenal growth in the demand of raw materials. This rise in demand has led to drastic changes the existing techniques of mining, food processing, power generation and other sectors where transportation of suspended solids play a major role. Due to this change, there has been an increase in requirements in slurry transportation.

Pump plays a vital role in transportation of slurry; different types of pumps are available for slurry transportation, but centrifugal pumps are most widely used in slurry transportation applications due to the following reasons:-

• Higher flow rates can be obtained.

• Pulse free flow can be obtained.

• Higher initial and maintenance cost of positive displacement pumps.

• Solid particle of any size can be transported.

Pump selection for slurry transport will depend not only on the flow, head required, suction conditions, type of installation and location, as for any other pump application, but also on the slurry flow regime and properties. Centrifugal or radial-flow type pump is the most commonly used in slurry service, are usually considered for the higher flow, lower head duties, whereas conversely, positive displacement reciprocating types is used for the lower flow, high pressure applications, e.g. long-distance pipelines. High pressures are also achieved with centrifugal pumps, depending on casing pressure limitations, by arranging

them in series. For slurry transportation, centrifugal pumps are usually cheaper, occupy less space and have lower maintenance costs than positive displacement types, and can handle much larger solids. Due to the particle impact on the blades of the pump, they cause erosion on the surface of the blade and reduce the life of the pump.

1.5 Centrifugal slurry Pump Materials

The material used for the pump must have:

- High Tensile Strength
- High Erosion resistance
- High Resilience
- High Fatigue Strength
- High Hardness
- High Corrosion Resistance

Pumps and their various components are made up of a number of different materials. Media type, system requirements, and the surrounding environment all are important factors in material selection.

Some materials used are described below.

- **Cast iron** provides high tensile strength, durability, and abrasion resistance corresponding to high pressure ratings.eg. White cast iron with 40% Cr.
- **Steel and stainless steel alloys** provide protection against chemical and rust corrosion and have higher tensile strengths, corresponding to higher pressure ratings. e.g. Type 316 Stainless Steel , Type 420C Stainless Steel, Ni-Hard, 13Cr4Ni, 16Cr5Ni, Ni – Cr – Mo Steel, 27 Cr-0.4 C5 Stainless Steel.
- **Other materials Aluminum, Brass, Bronze, Ceramics, Nickel alloys are also use in pump.**

Among all the options stainless steel 316 and stainless steel 420 are most widely used in pump industry. Stainless steel 316 is an austenitic stainless steel having excellent corrosion and erosion resistance in reducing media. The molybdenum present in stainless steel 316 increases its resistance to pitting corrosion. The alloy has good mechanical properties;

however its low hardness gives it a low erosion resistance. Stainless steel 420 is a martensitic stainless steel having a combination of high hardness and good general corrosion and erosion resistance. The alloy is machined in the annealed, or as cast condition and is subsequently hardened for service.

1.6 MOTIVATION OF THE PRESENT WORK

Pumping system is widely used in the transportation of coal, coal ash, iron ore, mineral concentration, and sewage sludge. In many of these applications, Transported slurries are complex multi-species mixtures containing solid with different densities and particle size. Several studies were dedicated to the effect of particle size in single species slurries on pipeline flow. The slurry from the bottom ash system as well as from fly ash is discharged by pipeline to the slurry pump. Centrifugal pumps are usually used for pumping the slurry through pipeline. In this we use the slurries having different particle size, density, viscosity, flow rate etc and measure the erosion characteristics of the centrifugal pump. The objective of the work is to investigate the erosion of the centrifugal slurry pump handling water and slurry experimentally in the slurry pot tester TR-41 at different speed and calculate the physical and chemical properties of ash like particle size distribution, static settle concentration, pH value and viscosity. Also numerical simulation of pump material erosion with or without coating handling ash is evaluate with different concentrations i.e. 20%, 30%, 40% and 50% (by weight) at 1150,1300 and 1450 r p m.

CHAPTER 2
LITERATURE REVIEW

2.1 NUMERICAL INVESTIGATION OF EROSION WEARS OF PUMP MATERIALS.

Hawthorne (2001) evaluated slurry erosion on different materials by Corioli's tests. Slurries consisting of glass beads of size 90-200μm size with 10% slurry concentration were taken and tests were performed on 1020 steel and copper at different impingement angles of 20°-90°. It was also observed that in slurry jet testing, most particles impact the specimen above its critical velocity resulting severe plastic deformation. In contrast, in the Corioli's test most particle impacts result in only elastic deformation or mild plastic deformation. Hence, elastic as well as plastic properties of specimen materials affect their performance in a Corioli's slurry erosion evaluation, thus the results obtained from Coriolis tests were more accurate.

Zhou et al. (2003) simulated the three-dimensional internal flow in three different types of centrifugal pumps (one pump has four straight blades and the other two have six twisted blades). A commercial three-dimensional Navier-Stokes code called CFX, with a standard k-ε two-equation turbulence model was used to simulate the problem under examination. In the calculation, the finite-volume method and an unstructured grid system were used for the solution procedure of the discretized governing equations for this problem. The computations are performed on a centrifugal pump with four straight blades (M1), a centrifugal pump with six twisted blades (M2), and a centrifugal pump with six twisted blades of different sizes (M3). The boundary conditions, at inlet constant mass-flow rate were specified at the inlet of the calculation domain for each computation. Various mass-flow rates were specified so as to study design and off-design pump conditions. Two rotational speeds 2900 r p m and 1450 r p m were used in the computations for both the straight-blade and the twisted blade cases. It was found that the predicted results for pumps M2 and M3 were better than those for pump M1, which suggests that the efficiency of pumps M2 and M3 will also be higher than that of pump M1.

Wood et al. (2004) analyzed the predicted and experimental erosion estimates in slurry ducts. Computational models for the impact velocity and impact angle in a bend have been successfully applied to the flow field and validated by electrical resistance tomography (ERT) to confirm the position of particle burdens. Predicted erosion damage levels and locations are compared to non-destructive ultrasonic and gravimetric measurements as well as wall thickness measurements made with a micrometer after cutting the pipe and bends sections. CFD code 5.4 with an embedded multi-phase (algebraic slip) model was used. A bend of 0.078m bore diameter and Rc/D ratio of 1.2 with a 0.078 m bore diameter straight pipe section 0.56 m in length located directly upstream of the bend was modeled. Both liquid and solid entry velocities were set to $3ms^{-1}$ with a uniform solid distribution. A standard k–ε turbulence model was used with standard wall functions and zero roughness.

Badr and Habib (2005) investigated the erosion in a pipe with sudden contraction. The flow was either in direction of gravity (down flow) or against it (up flow). The investigation follows the Lagrangian approach in which two mathematical models were used for the determination of the fluid velocity field and the solid particle trajectory and an erosion model was used to predict the erosion rate. The influence of the different parameters such as the inlet flow velocity (3–10 m/s), the particle diameter (10–400 μm), and carrier fluid is water at 20°C. The Lagrangian particle tracking is applied to calculate erosion of the protruded pipe. Flow simulation is obtained by using a CFD code 6.0. The flow velocity in the large pipe ranged from 1m/s to 10m/s and the particle size ranged from 10μm to 400μm. In these ranges, the results showed the strong dependence of erosion on both particle size and flow velocity but with little dependence on the direction of flow. The effect of flow direction was found to be significant only for large particle size (400μm) and moderate flow velocity (5 m/s). The erosion critical area was found to be the inner surface of the tube sheet (connecting the two pipes) in the region close to the small pipe inlet.

Asuaje et al. (2005)simulated a 3D-CFD of impeller and volute of a centrifugal pump using CFX code. The pump has a specific speed of 32 (metric units) and an outside impeller diameter of 400 mm. A structured grid was created using the CFX-Turbo grid software. For all simulations, the boundary conditions are as follows. At Inlet, total pressure applied in the rotation axis direction. Outlet imposed mass flow, symmetry surfaces positioned in the

middle of the blade passage; wall is taken as general boundary by default. The models $\kappa - \varepsilon$, $\kappa - \omega$, and SST were evaluated in the impeller flow simulation, under similar conditions and for the nominal flow rate of the pump. The volute-casing skeleton was imported by the preprocessor of CFX-5 to build the surfaces and volumes of the volute. After this process was conducted, the grid generation was completed. Extended inlet duct grid- Unstructured 104 973 nodes, Impeller grid -Structured 355 225 nodes, Volute casing grid -Unstructured 217 753 nodes, Inlet Total pressure = 101 325 Pa, Interface duct / impeller -Frozen rotor, Interface impeller / volute - Frozen rotor, Outlet - Mass flow, Turbulence model $\kappa - \varepsilon$, Discretization - Second order , An integral procedure for the optimization of centrifugal pumps has been developed based on 3D quasi-unsteady flow simulation using CFX-TASC flow and CFX 5.5 codes.

Brown (2006) evaluated the cause of erosive failures in slurry piping on the discharge of digester vessels at Alcoa's Wagerup alumina refinery by using CFD modeling. The commercial package CFX-5.7 is used to predict the motion of caustic liquor and bauxite particles through this system using an Eulerian-Lagrangian approach in conjunction with the k-ε turbulence model, and an erosion map is developed using the Finnie erosion model. The bauxite particles have high silica content and are hence highly abrasive. The digester outlet model was discretized using an unstructured tetrahedral mesh comprising of approximately 700,000 elements. Results from the model predict an accumulation of particles on the wall of the bend at the centre of a slow-moving vortex, and an associated high wear zone, the location of which is in excellent agreement with the observed wear on the plant.

Shah and Jain (2007) investigated the erosion rate coiled piping during fracturing slurry flow. The non-uniform wall erosion is caused by the centrifugal forces when pumping slurries at high rates. The slurry used in the experiments was prepared in 4.2 kg/m^3 guar as base fluid. The triplex pump can deliver fluid at a rate of $0.8m^3$/min with a maximum system pressure of 3.447×10^7 Pa. The ultrasonic thickness gauge was used to monitor the reduction in thickness of the tubing wall. The calculations of erosion rate by implementing a set of semi-empirical equations in commercial CFD software. The generalized erosion prediction procedure can be divided into three parts: flow modeling, particle tracking, and erosion calculation. In flow modeling, the coiled tubing model and the computational mesh generated

in the available pre-processor GAMBIT. For non-Newtonian fluids a modified form of the k–ε model known as the modified Lam–Bremhost model was used. In particle tracking, the code uses a Lagrangian particle-tracking algorithm that numerically predicts individual trajectories of a dispersed phase (solid particles, bubbles, etc.) through the flow field. It is found that erosion phenomenon in coiled tubing is highly non-uniform with tubing extrados (external radius) being more susceptible to erosion as compared to intrados (internal radius).

Thin et al. (2008) analyzed the centrifugal pump by using a single-stage end suction centrifugal pump. In centrifugal pump, water enters axially through the impeller eyes and water exits radially. The pump casing is to guide the liquid to the impeller, converts into pressure the high velocity kinetic energy of the flow from the impeller discharge and leads liquid away of the energy having imparted to the liquid comes from the volute casing. A design of centrifugal pump is carried out and analyzed to get the best performance point. The design and performance analysis of centrifugal pump are chosen because it is the most useful mechanical Rotodynamic machine in fluid works. The head and flow rate of this pump are 10 m and 0.179m^3/s and the motor speed is 2900 r p m. The low specific speed is chosen because the value of specific speed is 100. The number of impeller blade is 9 blades. The performance analysis of centrifugal pump is carried out after designing the dimensions of centrifugal pump. So, shock losses, impeller friction losses, volute friction losses, disk friction losses and recirculation losses of centrifugal pump are also considered in performance analysis of centrifugal pump.

Sahu et al. (2009) investigated the accuracy of numerical modeling of the laminar equation to determine the friction factor of pipe. The application of momentum equation is used to evaluate the friction loss coefficient. It uses the finite volume method to solve the governing equations for a fluid. It provides the capability to use different physical models such as incompressible or compressible, in viscid or viscous, laminar or turbulent etc. Geometry and grid generation is doing GAMBIT. The k- ε turbulence model is used according to Reynold number. The numerical differential equation is iterated and converged through the CFD where the friction factor is found to be .0151 at the entrance length of 2.7068 m. The experimental result show the friction factor is .0157 .The degree of accuracy of the numerical solution is checked with the experimental work done. This examination results indicates that

the proposed model can be used with the highest degree of accuracy to determine the friction factor in comparison to the other methods.

Graham et al. (2009) evaluated experimental and CFD results of erosion of two phase flow geometries. The working suspension is water with 7% by volume of silica sand. Two flow geometries were used: A 1.5x diameter pipe elbow. A bluff body extending over half of pipe diameter in cross flow. The commercial CFD code ANSYS CFX® was used to calculate the fluid velocity field, particle trajectories and consequent erosion for the cylinder in pipe case. The steady-state non-buoyant incompressible flow field was solved using a 3D unstructured mesh, with a k-ε turbulence model under the assumption that both the inlet velocity field and particle distribution were both uniform pipe diameters upstream of the sample. Particle tracking was performed using the standard transport model in CFX with turbulent dispersion, and 500,000 particles were released in random uniform distribution at the inlet at zero-slip velocity. Both the Finnie and the Grant and Tabakoff models are used to predict the local erosion rate as a function of the particle impact rate, velocity and angle based upon empirical correlations. It can be seen that both methods give similar results with most erosion occurring for this case towards the exit of the elbow.The CFD results also show good agreement with experiment. The Coordinate Measuring Machine (CMM) technique shows significant promise for obtaining quantitative data for comparison with CFD modeling of erosion.

Wang et al. (2009) evaluated the experimental data with different erosion models of CFD for slurry jet flows. In the experiments, four different parameters, viz. the impingement velocity, impingement angle, sand concentration and properties of target materials were varied. Their effect on the total weight loss and the erosion patterns are investigated. Experimental studies show that total weight loss has a power-law relation with respect to impingement velocity or sand concentration. The CFD approach for the modelling of the erosion process, generally, includes three main components: the hydrodynamic flow model, the particle tracking on the established flow field and the mechanistic erosion model. The establishment of the turbulent flow field can be realized by solving the Reynolds averaged Navier-Stokes (RANS) equations under suitable boundary/ initial conditions. The ability of the CFD model to predict the single-phase flow field has been well established. CFX4 is a finite volume algorithm based on a structured mesh that accepts a body-fitted coordinate system and provides a multi-

block facility. The total number of cells was varied from 12,600 to 110,000.Comparison of experimental data with various erosion models used in conjunction with CFD model provides a measure of goodness of fit.

Mittal et al. (2009) investigated the design of a centrifugal impeller for oil cooling blower system using computational fluid dynamics. Computational flow analysis of an axial–centrifugal flow system used for transformer oil cooling in WAP-5 and WAP-7 electric locomotives of Indian Railways. This leads to development of high centrifugal stresses causing hairline cracks to appear on the impeller rim at the blade–back plate joints near the impeller outlet after a few years of service. The centrifugal impeller is made of aluminum alloy and weight 34 kg. It has an outer diameter and a width of 710 and 254mm, respectively, with six vanes. Geometric model of the OCB (oil cooling blower) system is developed in the pre-processor GAMBIT. Tetrahedron elements were used for the impeller. Hexahedron- and prism-type elements were used for the enclosure. The commercial computational fluid dynamics code Fluent was used for the numerical simulation of the flow system. A standard k–ε turbulence model was employed for turbulence modelling. It is seen that the flow area first decreases and then increases non-linearly with the impeller rotation for fluid flow towards the impeller outlet. The weight of the impeller has also reduced from 34 to 32 kg. Also impeller tip speed is reduced from 108.18 to 99.9 m/s.

Spence et al. (2009) investigated the pressure pulsation during the operation and performance of centrifugal pump. The multi-block, structured grid CFD code TASC flow has been used to investigate the time variation of pressure within a complete double entry, double volute centrifugal pump. Three flow rates were investigated and the pulsations were extracted at 15 different locations covering important pump. This study also compared the pressure pulsations from the numerical analysis at locations within the impeller, volute and leakage flow passages with experimental test data and reasonable agreement was found. The pump operates at a speed of 1400 r p m, with a duty flow condition of 550m^3/h. The numerical simulation is conducted using CFX-TASC flow, which utilizes a finite element based finite volume method to solve the unsteady three-dimensional Navier–Stoker equations on a structured grid. Each component contain 10,000 to 85,000 elements so total grid elements of the whole pump were become 391,848. Turbulence was modeled with a standard

k-epsilon model; wall functions based on the logarithmic law were used. Large pulsations in the pump cause vibration and noise and the aim would be to reduce hydraulically generated noise and vibration by reducing the overall level of pressure pulsations in the pump.

Xing et al. (2009) analyzed the location and process of wear in two phase flow in centrifugal pump.The diameters of coal particles are 2.5μm and 10μm respectively.The load velocity of coal particles are defined as 3m/s and 5m/s, and the invasion angle is 90° and 15°, respectively. The artificial volume viscosity is 1.0, time step factor is 0.9, and calculation time is 3×10^{-6} s and 5×10^{-5} s, respectively. The results are consistent with the real wear situation. On this basic, base on the geometry non-linear theory and material non-linear theory, the wear process on flow components was simulated by ANSYS. The simulation results showed that there will be pits on the surface of flow components due to the impacting of coal particles with certain diameter, shape, impacting velocity and invasive angle; and the largest Von Mises stress will be at the pits. The distortion degree of pits and the largest Von Mises stress will increase with the increasing of coal particle diameter, impacting velocity and invasive angle, and with the decreasing of tip angle. The main locations of wear on the impeller of centrifugal slurry pump are in turn the impeller vane outlet and inlet, the intersect point of vane inlet with the rear cover plate, internal surface of rear cover plate, the middle of vane.

Ferng et al. (2010) studied the erosion-corrosion behavior of pipe in the nuclear power plants. The flow condition within the selected piping systems belongs to the single-phase flow and uses Standard k−ε turbulent model.A multi-block mesh system is employed to generate the meshes in the selected piping systems. A structured block is generated near the wall surface in order to reduce the deviation of velocity distribution and an unstructured mesh is used in the core of the pipe.

$$\text{Wwall thinning} = -0.1123 - \frac{7.36\times10^{-3}\ln(\text{TKE})}{\text{TKE}^2}$$

The amount of wall thinning decreases as the Turbulence kinetic energy (TKE) increases.The convergent criteria for the simulations are set as that summation of the relative residual in the control volumes for each governing equation is smaller than 10^{-5}.At the higher TKE portion, the amount of wall thinning decreases as the TKE increases. In the higher TKE or velocity gradient portion, the amount of wall thinning decreases as this hydrodynamic parameter

increases.This estimation model can simply predict the possible distributions of severe EC wear sites and subsequently assist the plant staff to schedule the pipe wall monitoring program in the measured range of pipe wall for the fittings.

Vijiapurapu and Cui (2010) studied the performance of turbulence model for rough pipes. Gridgen is used to generate the structured meshes where the first grid point is specified very close to wall (Y+ = 1.0). The Reynolds-averaged Navier–Stokes (RANS) equations were solved along with turbulence models, namely k−ε, k–ω, Reynolds stress models (RSM), and filtered Navier–Stokes equations along with Large Eddy Simulation (LES) to study the fully-developed turbulent flows in circular pipes roughened by repeated square ribs with various spacing. Friction factor is taken as 0.0165 and Reynolds number is 10000. The time-averaged k−ε, k–ω, models are capable of accurate quantitative calculations of the steady flow field with the least effort. RANS simulations benefit from the relatively low computational costs involved. In this approach, assemble average flow variables are computed and all turbulent fluctuations are modeled with a turbulence model. LES simulations on the other hand resolve the large scales of turbulence and are modeling only the smallest scales, which tend to be more universal and hence easier to model. These simulations have much greater success in predicting detached flows but result in much higher computational cost. Compared to the RANS models, the LES predicts both steady and instantaneous phenomena, but has severe computational cost.

Maitelli et al. (2010) simulated three-dimensional flow of centrifugal pump in the commercial software ANSYS® CFX® release 11.0. Turbulence model κ – ε and wall with no slip is used. The impeller rotational speed was set at 3500r p m. For each condition (C1, C2, C3), ten (10) flow rates were simulated. Three conditions were tested for the calculation of the pressures and the total head: the first condition was the impeller simulation with the blades length equivalent to the real model (C1); the second option was tested for the condition of complete connection of pump, impeller and diffuser, with the real blades length (C2); in the third option (C3), the impeller and the diffuser had their external radii increased by 4 mm. The meshes were generated by ANSYS 11.0 with wedge elements, pyramid elements and tetrahedral elements in a non-structured mesh, which is more appropriate to discretize irregular geometries. The boundary conditions were set as follows: a total uniform

pressure of 1 atm at inlet and variable mass flow rate at outlet.The results obtained with the simulations for the head characteristic curves (head versusflow rate) for the three conditions tested (C1, C2, C3), compared with the manufacturer´s data. The curves obtained from CFD model show a same tendency of behavior for the three cases in study. It can be observed that, for the smallest flow rates, there occurs an excessive head increase. This phenomenon happens because the diffuser is not considered in the simulation.

Minggao et al. (2010) studied the performance prediction for centrifugal pumps mainly based on numerical calculation. To make an improvement of numerical calculation method and performance prediction for centrifugal pumps, performance of six centrifugal pump models at design flow rate and off design flow rates, whose specific speed are different, were simulated by using commercial code fluent. The standard k-ε turbulence model and SIMPLEC algorithm were chosen. The simulation was steady and moving reference frame was used to consider the impeller-volute interaction. The characteristic prediction model for centrifugal pumps is established according to the simulation results. The head and efficiency of the six models at different flow rates are predicted and the prediction results are compared with the experiment results in detail. The comparison indicates that the precision of head and efficiency prediction are all less than 5%. The flow analysis indicates that flow change has an important effect on the location and area of low pressure region behind the blade inlet and the direction of velocity at impeller inlet. The study shows that using fluent simulation results to predict performance of centrifugal pumps is feasible and accurate. The method can be applied in engineering practice.

Kruger et al. (2010) investigated the erosion pattern of impeller resulting from experiments and simulation. In CFD program either apply particle tracking methods or perform multiphase flow computations to determine the impact of solid particles on the pump. The erosion tests are performed with quartz sand having density of 2610 kg/m^3 and particle size taken as 32μm. The fluid and solid phases are well mixed at the pump inlet. In boundary conditions average static pressure is imposed at outflow condition. At the walls, no-slip condition for the fluid phase and free slip condition for particle phase are applied. The mesh consists of 3238372 hexahedral elements. They studied the influence of parameters like particle concentration, impingement angle, particle velocity, turbulent kinetic energy, and vortices secondary flow structures on the

erosion pattern and correlates these parameters. It is clearly demonstrated that particle impingement angle and solid concentration play a dominant role in shock like processes as they occur along the leading edge of an impeller blade, impeller trailing edge, tip clearance and side plate. Contrarily, the flow pattern has a large impact on friction-like erosion processes as they occur along the blade, impeller trailing edge, tip clearance and side plate.

Tan et al. (2011) simulated the solid-fluid multi-phase flow problem in concrete pumping process. Discrete element method (DEM) was used to describe the trajectory of particles and interactions between the particles or between particles and wall. The length of the horizontal pipe is 1.6 m, the length of the vertical pipe is 0.6 m, and the bend section consist 90 degree circular bend with an outer radius of 0.4 m and inner radius of 0.3 m. The motion of the continuous fluid phase was evaluated by a Navier–Stokes solver, and a pressure gradient force model was adopted to calculate the solid–fluid interaction force. Collocated grid was used to arrange fluid variables in center of a fluid computational cell, and the whole computational domain was divided by 2000 structured hexahedron CFD cells, Patankar's SIMPLE algorithm was adopted to compensate the pressure. The wear pattern in an elbow depends on the magnitude of the interaction forces and the frequency of interactions between particles and wall. The highest pressure is found along the extrados farthest from the center of curvature while the lowest pressure is along the intrados nearest to the center of curvature. The wear pattern in an elbow depends on the magnitude of the interaction forces and the frequency of interactions between particles and wall. Through the simulation, the maximum erosion was observed at 30–40 degree of the outer wall of the elbow, which has a good agreement with that observed in real case.

Majid et al. (2011) studied the experimental and computational failure analysis of natural gas carbon steel pipe. SEM is used for checking the microstructure of pipe material. In experimental set up slurry is pump through the pipe. Water is taken as fluid. The mesh is constructed using GAMBIT mesh generation routine. The multiblock-structured-unstructured hybrid mesh was adopted for the test rig model whereby the unstructured mesh was used in regions surrounding the test specimen whilst the structured mesh was imposed to other regions. The test rig model utilizes 49156 nodes, 147082 faces and 48918 cells of discredited domain. The inlet pressure was fixed at 1000 kPa. In computational approach Fluent 6.2 was

used to investigate the jet flow pattern and erosion behavior on the pipe sample. The equations employed are the Reynolds Averaged Navier–Stokes Equation together with other equations describing related phenomena under investigation. The turbulence characteristics are assumed to follow the k−ε turbulent model. k– ε turbulence model is chosen due to its frequent validation of its turbulence model and has been used widely in industrial related flow problem. CFD simulation results indicated that the highest strain rate region occurs above and below the impact point which corresponds directly to the failure region found from the experimental study.

Song et al. (2011)investigated the performance of jet pump using commercial software ANSYS CFX with two classical types. This jet pump is designed to transport water with lots of sand particles. Type A has an axial nozzle in the center where a primary driving fluid is injected, and the suction nozzle is on the side. Type B has an annular suction nozzle on the outside and the inject nozzle in the center where a primary driving fluid is injected. Type C is the newly designed jet pump, where the suction nozzle is axial and the primary driving fluid is injected through an ‘‘L’’ shape pipe like an elbow. They used CFD model ANSYS for comparing the performance and to determine the erosion wear at different position he assumed that the flow is turbulent flow. So Navier–Stokes Equations (RANS) are utilized to deal with the turbulence flow. Grid generation was done in ANSYS ICEM –CFD about 300,000 nodes of quadrilateral mesh were used for each model. The particle velocity was assumed to be identical to the water velocity at both inlet and suction. A particle mass flow of 0.04 kg/s was specified at the inlet. The maximum sand erosion rate density of approximate 932 kg (m^2 /s) is predicted at the end of the bended pipe, the sand particles concentrate and impact at the suction chamber and diffuser is less as compared with the bend of the pipe. The results show that the newly designed type of jet pump has the best performance in mass flow ratio, pressure ratio and efficiency compared with the classical types under the specified/designed working condition, which is the most important factor concerning its usage. The new type of jet pump has rapid sand erosion due to the bended pipe. That can be very useful for the prevention of erosion.

Neifei et al. (2011) implemented Reverse Engineering (RE) and numerical simulations of Computational Fluid Dynamics (CFD) to study the centrifugal pumps with splitter blades.

According to the thought of RE, they measured centrifugal pump with splitter blades for point cloud data utilizing optical scanner, and then imported the point cloud data into CATIA. Finally, CATIA was used to achieve the reverse modeling of the part. The three-dimensional geometric model of centrifugal pump CFD simulation is the flow channel of pump. Meshing was done by using Gambit. Turbulence model selected the standard K-ε model. In this process, the law of velocity and pressure distribution of internal flow about the centrifugal pump with splitter blades is preliminary disclosed. In addition, performance prediction was carried out in centrifugal pumps. Comparing to the calculation curve and text characteristic curve, it's obvious that simulation results are in good agreement with experimental results. The results verify the reliability and feasibility of the research method.

Zhou et al. (2012) presented the three-dimensional flow field simulation of a centrifugal pump by using commercial CFD code. In order to study the most suitable turbulence model, the three known turbulence models of Standard k-ε, RNG k-ε, Realizable k-ε were applied to simulate the flow field of the centrifugal pump and predict the performance of the pump. Velocity-inlet boundary condition is used for inlet.Outflow boundary condition is used for outlet. Outer walls are stationary but the inner walls are rotational. There are interfaces between the stationary and rotational regions. The simulation results of head and efficiency were compared with available experimental data, and the comparison showed that the result of the numerical simulation by RNG k-ε model had the best agreement. Additionally, the effect of number of blades on the efficiency of pump was studied. The number of blades was changed from 4 to 7. The blade number increase, both pressure and velocity distribution trend to be more even and to some extent there is a positive effect on efficiency and performance. The results showed that the impeller with 7 blades had the highest efficiency.

Zhang et al. (2012) simulated erosion and particle motion of multi- medium Oil -Coal-Water slurry Pump. Oil-coal-water slurry as a new alternative fuel was used on diesel engines. The Multi medium oil-coal-water slurry pump wears serious bottleneck with presence of solid coal particles.Three-dimensional model is made of Oil-coal-water pump fuel injection into gambit. Pump fluid regions are divided into 116261 grid cells. According to characteristics of piston plunger motion and conservation of mass law, speed, inlet pressure or inlet flow rate, etc are obtained from inlet boundary conditions. In numerical simulation, piston pump

working process is compression. Outlet boundary condition can give exit. Based on VOF multi-flow model, Reynolds stress model and discrete phase model to the continuous phase and dispersed phase, the multi- medium erosion and motion trajectory of solid particle the impact progress between solid particle and machine surface were simulated successfully. According to the simulation result, the related parameters of solid particle, such as density and diameter, mix proportional and plunger speed of impeller greatly influenced the motion trajectory and the impaction with machine surface of solid particle. By contraries, little particle was liable to impact the plunger barrel assembly. The plunger speed more high, the plunger barrel assembly more erosion. The plunger barrel assembly wears with solid mix proportional.

Wong et al. (2012) performed combined experimental and computational study to examine and predict the erosion characteristics on a simple flat aluminum plate, with a central hole, that is impacted with silica sand. In the oil and gas and other process industries it is necessary to have accurate and versatile methods of determining surface erosion rates, and to use them to predict the erosion of surfaces over time. Silica sand with 80% used between 150 and 350 μm, and a median diameter equal to 223 μm; density = 2650 kg/m^3. The simulation was performed using the commercial software ANSYS CFX-12, which solves the Reynolds averaged Navier–Stokes equations. The model used an isothermal, steady state, single phase Eulerian simulation to represent the air flow, while simulation of sand particles was performed using Lagrangian particle tracking techniques. This sub-model was then incorporated into a computational fluid dynamics environment to predict erosion on the flat plate. It was found that profile development on bluff surfaces could be predicted with accuracy generally much less than a nominal maximum deviation of 30%. Erosion of the more complex aspects of the geometry was only qualitatively predicted. The importance of allowing for the erosion incubation period in calculations is demonstrated, and methods for improving erosion prediction of complex geometries are discussed.

2.2 EROSION WEARS OF PUMP MATERIAL WITH OR WITHOUT COATING.

Ping et al. (2005) analyzed the failure of impeller of slurry pump used in zinc hydrometallurgy process. Zinc hydrometallurgy process involves roasting, leaching, purification, electrolyte deposition, melting into zinc ingot and so on, in leaching process a

number of slurry pumps are used to transport solid–liquid mixed slurry containing $ZnSo_4$ particles, silica and diluted sulfuric acid and so on to a filter to be purified. The temperature of the slurry solution is about 70 °C, the density of that is 1.681 g/l, the mass ratio of liquid to solid for the slurry is about 8:1 and its pH value is about 3. The failure of the impeller of slurry pump initiated from the serious corrosive wear. Failure analysis revealed that an improper austenite/ferrite ratio of duplex stainless steel (DSS) material resulting from too high nitrogen content was primarily responsible for the rapid failure of the impeller. In addition, a melting test in a vacuum furnace verified again that nitrogen content had a significant effect on austenite/ferrite ratio of duplex stainless steel; a comparing corrosive wear test revealed further that DSS consisting of equal austenite/ferrite volume showed better corrosive wear resistance. Corrosion is in a subordinate position, but erosion takes up a dominant position in total erosion wear volume. Too high nitrogen addition in the duplex stainless steel (DSS) resulted in too low ferrite content, as a result of too short service life; a recommended nitrogen content value is 0.1–0.3%. SEM micrographs is used for analyze the steel. The result of simulated corrosive wear test indicated that DSS possessing almost equal ferrite and austenite volume showed better corrosive wear resistance.

Tabakoff et al. (2006) analyzed experimental and analytical studies of erosion and deposition in turbomachines by ingested particles and the associated performance loss. Experimental investigations of particle-surface interactions in special tunnels that control particle impact conditions provide blade and coating material erosion and particle restitution characteristics. The results of erosion studies often express the ratio of surface mass or volume removal to impinging particle mass. In general the erosion rate of a given material is affected by the particle's impact velocity and impingement angle. The variation of erosion rate with impingement angle is characteristically different for ductile and brittle material. Both experimental and numerical studies were conducted to determine the pattern and intensity of compressor and turbine-blade erosion. The increased tip clearances and changes in airfoil shape cause by erosion to turbomachinery causes performance deterioration. In turbines, inertial impact at high velocities of particles larger than a few microns in diameter on airfoil leading edges and pressure surfaces can cause erosion or deposition depending on the balance of hard versus molten particles. Deposition is expected to become more important in the first stage of turbine hot sections as turbine inlet temperatures increase due

to the higher fractions of molten particles. Increased fuel consumption, decreased efficiency, flow capacity, and reduced power and surge margins have been attributed to fan and compressor erosion.

Ariely et al. (2006) analyzed the failure of an impeller of pump of cyclic cooling water system of power plant. Tolyltriazole (TT) is included in the water as corrosion inhibitor. SEM, EDS and Metallography were used to analyze the impeller failure. Most of the surface of both blades was pitted, and clear grinding marks were noticeable. The pits are horseshoe-shaped. Examination of those pits revealed a pattern of dendrites on the pit's surface. Cross-section shows that the pits are craters like, which is typical to pits that are formed by impingement. Corrosion, which follows impingement, roughens those pits surface. Those findings are typical to erosion–corrosion mechanism. Elements mapping of dendrite like pattern shows that the dendrite material is rich with copper, while inter dendritic material is rich with lead and tin. We conclude that in both blades open shrinkage defects were filled by weld followed by grinding. As a result, blade surfaces were defected causing local irregular flow regime which caused to preferred impingement of the welded material. The impingement bubbles were filled by TT vapors that, due to the relative low pressure, decomposed. One of decomposition products was ammonia, which caused the preferred corrosion of copper. The open shrinkage defects were exposed due to material removing by cavitation erosion corrosion process.

Santa et al. (2007) studied the slurry erosion of two coatings applied by oxy fuel powder (OFP) and wire arc spraying (WAS) processes onto sand-blasted 304 steel, and the results were compared to those obtained with 431 and ASTM A743 grade CA6NM stainless steels, which are commonly used for hydraulic turbines and accessories. The adherence of the coatings to the substrate was measured according to ASTM standard, while the microstructure and worn surfaces were characterized by optical and scanning electron microscopy. Slurry erosion tests were carried out in a modified centrifugal pump, in which the samples were placed conveniently to ensure grazing incidence of the particles. The slurry was composed of distilled water and quartz sand particles with an average diameter between 212 and 300 μm (AFS 50/70) and the solids content was 10 wt% in all the tests. The mean impact velocity of the slurry was 5.5 m/s and the erosion resistance was determined from the

volume loss results. The coated surfaces showed higher erosion resistance than the uncoated stainless steels, with the lower volume losses measured for the E-C 29123 deposit. SEM analysis of the worn surfaces revealed intense plastic deformation in both coated and bare stainless steels, with little evidence of brittle fracture in the microstructure. The measured adhesive strength of the coatings was considered acceptable for the processes employed.

Espitia et al. (2009) studied slurry and cavitation erosion resistance of six thermal spray coatings in laboratory and compared to that of an uncoated martensitic stainless steel. Nickel, chromium oxide and tungsten carbide coatings were applied by oxy fuel powder (OFP) process and chromium and tungsten carbide coatings were obtained by high velocity oxy fuel (HVOF) process. The microstructure of the coatings was analyzed by light optical microscopy (LOM) and scanning electron microscopy (SEM), as well as by X-ray diffraction (XRD). The cavitation erosion resistance of the coatings was measured in a vibratory apparatus and the slurry erosion tests were carried out in a modified centrifugal pump in which the samples were conveniently placed to guarantee grazing incidence conditions, as well as in a high velocity jet erosion testing machine. The results showed that the slurry erosion resistance of the steel can be improved up to 16 times by the application of the thermally sprayed coatings. On the other hand, none of the coated specimens showed better cavitation resistance than the uncoated steel in the experiments. The main mass removal mechanisms observed in all the coatings submitted to slurry erosion were micro-cutting and micro ploughing as well as detachment of hard particles. In cavitation erosion, OFP coatings showed brittle fracture and micro cracking, and in nickel-based coatings some ductile deformation was also observed. In HVOF coatings, detachment of small particles led to coalescence of pores in WC/Co coatings while in CrC coatings the main wear mechanism was brittle fracture of particles.

Zhenlin et al. (2010) studied the effect of SiC particles sizes on erosion wear behaviour of SiC/epoxy resin composite on self-made slurry erosion wear tester.The slurries were composed of quartz sand with sizes of 600-800 μm and water, and the ratio of quartz sand and water in slurry was 1:10. The slurrywas jetted to the surface of SiC/epoxy resin composite at speed of 11.1m/s and at different impact angle. The erosion test was running for 60 minute for each sample. The erosion wear rate of samples was taken as the weight loss per

minute. The wear surface morphology of SiC/epoxy resin composite was observed and analyzed by scanning electron microscope (SEM). The results show that the erosion wear rate of SiC/epoxy resin composite would be decreased with the increase of SiC particle sizes. With the increase of impact angle, the erosion wear rate would be increased first, and then decreased. It would be peak value when the erosion wear test was carried out at 60° impact angle. When SiC particles were mixed with different sizes, the erosion wear rate of SiC/epoxy resin composite would be lowest. The erosion wear mechanism of SiC/epoxy resin composite was analyzed by observation of worn surface morphology.

Wang et al. (2011) investigated the corrosion and slurry erosion–corrosion (E–C) behaviour of FeCrMoMnWBCSi amorphous metallic coatings (AMCs) compared with 304 stainless steel by static electrochemical measurements and weight loss tests under rotating conditions in simulated seawater. E–C rates of the AMCs increased with flow velocity, particle size, sand content and NaCl concentration. The AMCs are preferentially attacked at coating defects. The superior E–C resistance of AMCs can be attributed to the high microhardness, alloying elements and amorphous microstructure. The AMCs with better slurry E–C resistance may be good candidates to solve the E–C problems of marine pumps in sand-containing seawater.The E–C processes highly depend on flow velocity, sand size and sand content. The E–C rate of 304 stainless steel increases rapidly with flow velocity, sand size and sand content, whereas AMCs increases mildly. The E–C process is controlled by the mechanical damage resulting from erosion. 304 stainless steel exhibits a typical ductile erosion damage involving the extensive plastic deformation. AMCs are preferentially attacked from coating defects. The high hardness may be the main reason for the higher E–C resistance of AMCs relative to 304 stainless steel.The AMCs with better slurry E–C resistance may be good candidates to solve the E–C problems of marine pump in sand-containing seawater.

Liu et al. (2011) investigated the erosion wear behavior of WC-12Co coatings deposited by HVOF spraying.The erosion wear experiment system was developed to simulate the working condition to study the erosion wear properties. The corundum sand with main composition of Al_2O_3 and quartz sand with main composition of SiO_2 were used to investigate the effects of sand variety on the erosion wear properties.The wear loss per unit area of the coating eroded

by corundum sand is about 1.48 times as much as that eroded by quartz sand.The impact angle is 60°, tangential speed of abrasive particles mainly generates cutting and plowing effect, while vertical speed produces hammering effect. The higher is the impact energy, the more severe of the spalling of the WC particles, leading to higher wear loss of the coating.The results show that the failure mechanism of the coating eroded by corundum sand is cracking between WC grains, while for the coating eroded by quartz sand, the failure mechanism is microcutting and microploughing.

CHAPTER 3

PROPERTIES OF PUMP MATERIAL AND ASH

3.1 STUDY DIFFERENT PROPERTIES OF PUMP MATERIALS

Type 316 is an austenitic chromium nickel stainless steel containing molybdenum. This addition increases general corrosion resistance, improves resistance to pitting from chloride ion solutions, and provides increased strength at elevated temperatures. Typical uses include exhaust manifolds, furnace parts, heat exchangers, jet engine parts, pharmaceutical and photographic equipment, valve trim, slurry pumps, chemical equipment, digesters, tanks, evaporators, pulp, paper and textile processing equipment, parts exposed to marine atmospheres and tubing. SS 316 offers higher strength and better creep resistance at higher temperatures.

Type 420 stainless steel is a martensitic stainless steel having a combination of high hardness and good general corrosion resistance. The alloy is machined in the annealed, or as cast condition and is subsequently hardened for service. It is magnetic in both the annealed and hardened conditions. Maximum corrosion resistance is attained only in the fully hardened or fully hardened and stress relieved condition. It is never used in the annealed condition. Applications requiring good corrosion resistance and high hardness are ideal for this alloy. Typical uses include cutlery, surgical and dental instruments, scissors, slurry pumps, tapes and straight edges. The alloy is not normally used at temperatures exceeding 427°C due to rapid softening and loss of corrosion resistance.

3.1.1 Chemical composition

The chemical composition of stainless steel 316 and stainless steel 420 samples were determined by the spectrometer analysis as shown in figure 3.1.A spectrometer (also known as spectrophotometer, spectrograph or spectroscope) is a device that used to measure the chemical composition of ferrous materials.

The chemical composition is measured by the light intensity produced by arc. A spectrometer is used in spectroscopy for producing spectral lines and measuring their wavelengths and intensities. Spectrometer instruments operate over a very wide range of wavelengths, from gamma rays and X-rays into the far infrared. Figure 3.1, showing the spectrometer.

Figure 3.1 Spectrometer

Composition of both pump materials Stainless steel 316 and Stainless steel 420 are shown in the table below:

Table 3.1 Composition of Stainless steel 316 and steel 420

Name of the element (%)	Percentage average of steel 316	Percentage average of steel 420
Fe%	67.5	65.76
C %	0.180	0.148
Si %	0.443	0.959
Mn %	1.46	0.779
P %	0.0315	0.0358
S %	0.0307	0.00217
Cr %	18	12.15
Mo%	2.00	2.32
Ni %	9.26	0.164
Al %	0.0010	5.75
Co %	0.166	0.0687
Cu %	0.415	0.698
Mb %	0.0182	4.64
Ti %	0.0166	0.182
V %	0.0399	0.211
W%	.0673	.0768

3.1.2 Micro hardness

Microhardness testing is used for measuring the hardness of a material on a microscopic scale. A precision diamond indenter is impressed into the material at loads from a few grams to 1 kilogram. Constant load of 100gm was used for all specimens. The impression length, measured microscopically, and the test load are used to calculate a hardness value. The hardness values obtained are useful indicators of a material's properties.

The indentations are typically made using either a square-based pyramid indenter (Vickers hardness scale) or an elongated, rhombohedral-shaped indenter. The tester applies the selected test load using dead weights. The length of the hardness impressions are precisely measured with a light microscope using either a filar eyepiece or a video image and computer software. A hardness number is then calculated using the test load, the impression length, and a shape factor for the indenter type used for the test and the test specimen shown in Figure.

Figure 3.2 Microhardness Tester

Figure 3.3 and 3.4 shows the indentation mark on steels specimens. The area of the indentation is measured by the software by which the area hardness is calculated. Steel 316 shows the maximum hardness as compare to steel 420.

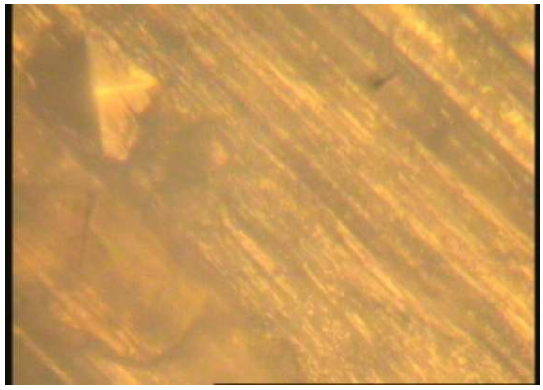

Figure 3.3 Indent mark on SS 316

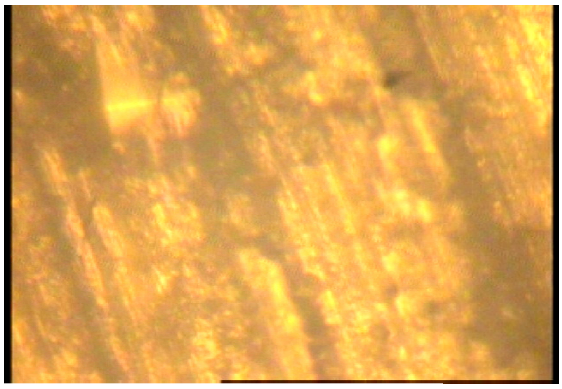

Figure 3.4 Indent mark on SS 420

Table 3.2 Microhardness of pump materials

Material	Hardness at a load of 100 gm.
Stainless steel 316	116 HRB
Stainless steel 420	102 HRB

Table 3.3 Mechanical properties of pump materials

Property	Steel 316	Steel 420
Density	8000kg/m^3	7800kg/m^3
Tensile strength	515 Mpa	860Mpa
Yield strength	205Mpa	-
Elongation percentage	40%	-

3.2 FLY ASH AND BOTTOM ASH PROPERTIES

Fly ash is one of the residues generated in combustion, and comprises the fine particles that rise with the flue gases. Ash which does not rise is termed bottom ash. In an industrial context, fly ash usually refers to ash produced during combustion of coal. Fly ash is generally captured by electrostatic precipitators or other particle filtration equipment before the flue gases reach the chimneys of coal-fired power plants and together with bottom ash removed from the bottom of the furnace is in this case jointly known as coal ash. Depending upon the source and makeup of the coal being burned, the components of fly ash vary considerably, but all fly ash includes substantial amounts of silicon dioxide (SiO_2) (both amorphous and crystalline) and calcium oxide (CaO), both being common ingredients in many coal-bearing rock strata.

Bottom ash is residue of coal, burning in thermal power plants. Bottom ash being heavier in size cant escapes up the chimney along with the fumes to the atmosphere whereas fly ash escapes up the chimney along with the fumes to the atmosphere. Bottom ash is coarser than fly ash with grain size spanning from fine sand to fine gravel. We must know the chemical composition of both fly and bottom ash. Chemical composition was measured by SEM. The

following tables will show the chemical composition. Different properties of fly and bottom ash like particle size distribution, static settled concentration, specific gravity and rheological behaviour are given below.

Table 3.4 Chemical composition fly ash

Element	Weight%	Atomic%	Compound%	Formula
C K	4.63	7.63	16.95	CO_2
Mg K	0.16	0.13	0.26	MgO
Al K	14.25	10.46	26.93	$Al_2 O_3$
Si K	20.39	14.38	43.61	SiO_2
K K	0.80	0.41	0.97	K_2O
Ca K	0.19	0.10	0.27	CaO
Ti K	2.83	1.17	4.72	TiO_2
Fe K	2.16	0.77	2.78	FeO
Cu K	1.58	0.49	1.97	CuO
Zn K	1.23	0.37	1.53	ZnO
O	51.78	64.10		
Totals	100.00			

Table 3.5 Chemical composition of bottom ash

Element	Weight%	Atomic%	Compound%	Formula
C K	13.20	19.33	48.38	CO_2
Mg K	0.13	0.09	0.21	MgO
Al K	8.01	5.22	15.14	Al_2O_3
Si K	12.93	8.09	27.66	SiO_2
K K	0.51	0.23	0.62	K_2O
Ca K	0.28	0.12	0.39	CaO
Ti K	0.97	0.36	1.62	TiO_2
Fe K	3.13	0.98	4.02	FeO
Cu K	0.83	0.23	1.03	CuO
Zn K	0.74	0.20	0.92	ZnO
O	59.27	65.14		
Totals	100.00			

3.2.1 Particle Size Distribution (PSD)

It refers to the variation in the size of solid particles present in the solid sample. To determine the distribution of particle size, two methods namely sieve analysis and hydrometer analysis is employed. For coarser particle size distribution i.e. above 75 µm sieve analysis is used whereas hydrometer analysis is used for finer particles i.e. below 75 μm. A known weight of representative sample of solid particles is taken and washed over a B.S. 200 mesh (75 μm). The material retained over the sieve as well as the finer particulate material are dried in an oven. The dried coarser material is sieved through a set of standard sieves. The dried coarser material is sieved through a set of standard sieves. Special care is taken to ensure that the sample is properly dried. The sample retained on each sieve is collected and the percentage retained on each sieve is calculated using the standard procedure. The experimental result of fly and bottom ash is shown in Figure 3.5.

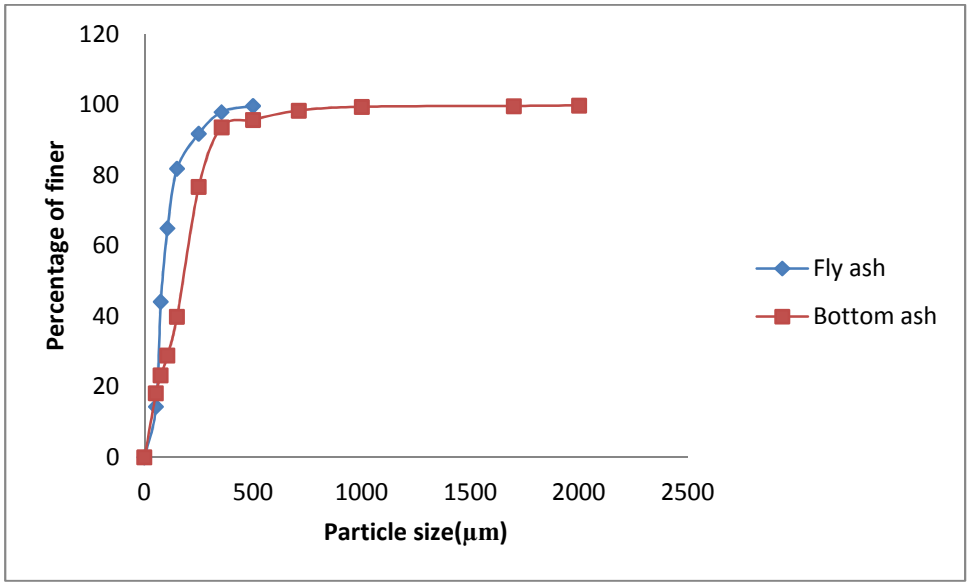

Figure 3.5 Particle size distribution

3.2.2 Static Settled Concentration

The static settled concentration is a very important parameter as it decides the highest limit of solid concentration, which can be achieved by gravitational settling. The static settled

concentration depends on a large number of parameters like specific gravity, shape and size distribution of solids, density and viscosity, of carrier fluid etc.

This value of solid concentration in the settled portion of slurry is the static settled concentration. The slurry level at regular intervals of time was also recorded during the process of settling of the slurry to determine the setting rate of the slurry. By following this procedure we found that as initial concentration of both fly and bottom ash was 20% by weight, final settled concentration after 5 hours comes out was 58.5%.

3.2.3 Specific Gravity Ash

The specific gravity of solid particles is determined using Standard Pyknometer Method. In this method first take 50 ml Pyknometer and clean it thoroughly, keep it in the oven in order to remove moisture from Pyknometer. After 2 hours, take out the Pyknometer from an oven and allow it to cool down, and then take the weight of Pyknometer (Wb). After weight put some solids (over dried) about 30 grams in it and weight it again and note down this weight (Wbs). After this slowly pour water (distilled) in the Pyknometer so that no air is entrapped in it and shake it well, and keep on pouring the water. Shake it well each time till all the solid get wet. Fill $3/4^{th}$ of bottle with water and put the thumb on the mouth of the bottle and shake it well for 5 minutes. Keep it for at least 2 hours, so that air bubbles get out from the bottle. Then fill the bottle of water and cork it. Clean it with cloth/tissue paper and weight it. Note down the weight (Wbsw). Now remove the solids from the bottle and clean it, Thoroughly, Dry it and fill it with distilled water. Note down the weight (Wbw).

3.2.4 pH VALUE

A pH meter was used for measurement of the pH value of the slurry of any given solid concentration. The electrode of the meter was first moistened with tap water and then calibrated with a buffer solution of a known pH value. It is cleaned by rinsing vigorously with distilled water and then immersed in the slurry sample whose pH value was to be determined. The pH suspension was read on the digital display unit when equilibrium value was reached. From the pH meter we found that pH value of both fly and bottom ash lies between 6 to 7.5 this shows that both are non reactive in nature.

3.3 RHEOLOGY

Rheology is the study of the flow of matter, primarily in the liquid state, but also as 'soft solids' or solids under conditions in which they respond with plastic flow rather than deforming elastically in response to an applied force. Study of flow properties of water and ash mixture is important for ash disposal system in the thermal power plants. The flow behaviour of liquids under applied stress is of great relevance in the field of engineering. A Non-Newtonian behaviour shown by solid-liquid mixture if solid added in carrier fluid beyond a certain limit. To establish the rheology of ash-water mixture, the variation of shear stress with shear rate has been obtained over a range of concentrations varying from 10 to 50% (by weight).

3.3.1 Rheological Measurements

The shear stress-shear rate relationship for fly and bottom ash slurry can be determined by using bob and cup geometry, stirrer and cup geometry of rheometer (make Anton paar). The geometry consists of a fixed cylinder (bob) and a rotating cylinder (cup). The slurry placed between the annular space between the two cylinders and a torque applied on the rotating cylinder (cup). The viscosity of slurry obtained by the graph plotted between shear stress and strain rate. Figure 3.6 showing the rheometer used for present investigation**.**Newtonian or Non-Newtonian behaviour of fly ash slurry has been identifies by measuring the variation of shear stress with shear rate over a range of concentrations. The shear rate given as an input in the rheometer and corresponding shear stress obtained as output. The fluid will show the Newtonian behaviour when the graph shows linear relationship between shear stress and shear rate and if it deviates from linear curve, fluid will show the Non-Newtonian behaviour.

Figure 3.6 Rheometer (Anton Paar)

The determination of Newtonian or Non-Newtonian behaviour of bottom and fly ash water mixture has been identified by measuring the variation of shear stress with shear rate at different concentrations. The shear rate is given as an input in the rheometer and corresponding shear stress is obtained. The linear relationship between the shear stress and shear rate graph shows that the fluid is showing the Newtonian behaviour and as it deviates from linear curve, fluid will show the Non-Newtonian behaviour. The table 3.6 -3.7 shows shear stress and shear rate at different concentrations. All samples of fly ash at different concentration give Newtonian behaviour. In case of bottom ash, 10% to 30% give Newtonian behaviour but at 40% to 50% give Non- Newtonian behaviour.

Table 3.6 Rheological Properties of Bottom ash

Concentration (Cw) %	Slurry viscosity (Pascal/sec.)	Shear rate 1/s	Flow behaviour
10	0.020433	690.48	Newtonian
20	0.02456	691.48	Newtonian
30	0.031036	691.48	Newtonian
40	0.07211	691.48	Non-Newtonian
50	0.06576	691.48	Non-Newtonian

Table 3.7 Rheological Properties of fly ash

Concentration (Cw) %	Slurry viscosity (Pascal/sec.)	Shear rate 1/s	Flow behaviour
10	0.00235	385.3	Newtonian
20	0.00667	385.3	Newtonian
30	0.007506	385.3	Newtonian
40	0.01156	385.3	Newtonian
50	0.03432	385.3	Newtonian

CHAPTER 4

EXPERIMENTAL EVALUTION OF EROSION WEAR OF PUMP MATERIAL WITH OR WITHOUT COATING

4.1 SLURRY POT TESTER

A rectangular sample under evaluation is made to rotate in a slurry cup. The sample is weighted before and after the test to determine loss of mass due to slurry erosion. Volume loss is computed for comparison, due to difference in densities of materials. Index of erosion is reported as loss of volume.

Figure 4.1 Erosion pot tester TR41

4.1.1 Preparation of slurry

Slurry pot tester is prepared on each slurry vessel, usually quartz, sand, ash and coal is preferred. Clean thoroughly slurry vessel. Weight and pour 600gms of ash in each vessel. Fill each vessel with 600gms of water.

4.1.2 Specimen preparation

Typical specimen is rectangular shape 25.4×76mm, 6.35mm thicknesses. The specimen should be smooth, flat, and free of scale, machined and ground to size with a central hole for

clamping. Remove all the dirt or foreign matter from the specimen. Clean the specimen with a solvent or cleaner or dry to remove all the traces of solvent.

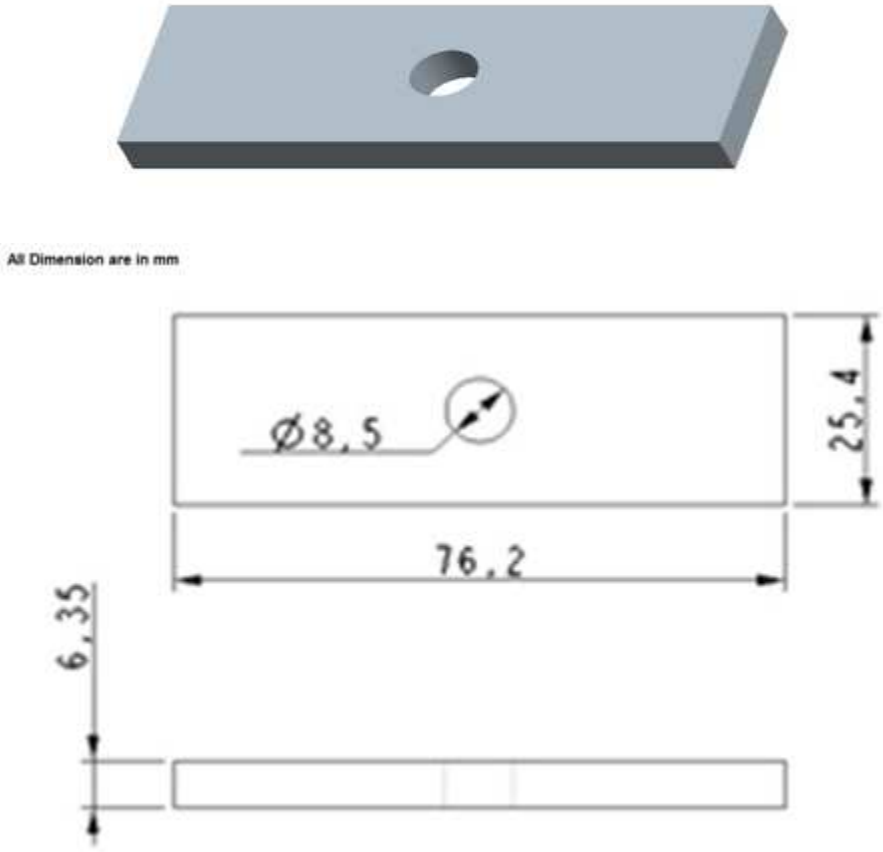

Figure 4.3 Sample Drawing

4.1.3 Test procedure for run in test

Clean and rinse the slurry chamber to remove the leftovers of slurry from the previous test.For 50% concentration of slurry,weight 600 gm of slurry and fill inside the slurry vessel.Fill vessel with 600gm of water.Weight specimen on weighing machine which has least counts 0.0001gm and record the value.Locate specimen on the slot of each spindle and tighten with stirrer.Connect inlet port to water source and outlet to drain.Switch “ON” MCB to supply power to tester to allow 1 min for stabilizing the circuits.Press start button on control panel and slowly rotate the set speed knob till the speed display module show 100 r p m.Press STOP to assets spindle rotation, but retain the position of set speed knob.Place the slurry vessel inside the water jacket.Clean the top surface of vessel and base plate with

cloth.Slowly rotate the handle to raise the water jacket till it presses the base plate with sufficient pressure to prevent leakage of the slurry.Set the test duration to 3 hrs to shut off automatically after completion of time,Press START switch to begin specimen rotation.Specimen rotates, the direction or rotation is clockwise the stirrer agitates slurry, the slurry rotates along the direction of rotation, the slurry rotation is arrested by vertical fins to propel it towards specimen.The motor will be switched OFF automatically after the elapse of the preset revolution.Clean the surface of each specimen with cloth to remove slurry.Allow the specimen to cool, to room temperature and remove from specimen holder.Rinse to clean and dry the specimen.Weight each specimen and compute mass loss.

Following parameters were taken while performing erosion wear on pump materials with or without coating.

Speed: 700, 1000, 1400 r p m

Concentration: 20, 40, 60% by weight

Time: 60, 90,120, 150min.

Ash: bottom and fly ash

Below figures show the effect of these parameters on pump material, we found that with the increase in speed, time and concentration the weight loss increases and chromium coating provides a better resistance for the material loss.

4.2 EROSION WEAR OF STAINLESS STEEL 316

Steel 316 rectangular specimen runs in pot tester at different speed, time and concentration to find out the erosion of the samples. Weighing machine used for the weight loss measurement before and after the test. Weighing machine has a least count 0.0001mg.

4.2.1 Effect of time, speed and concentration

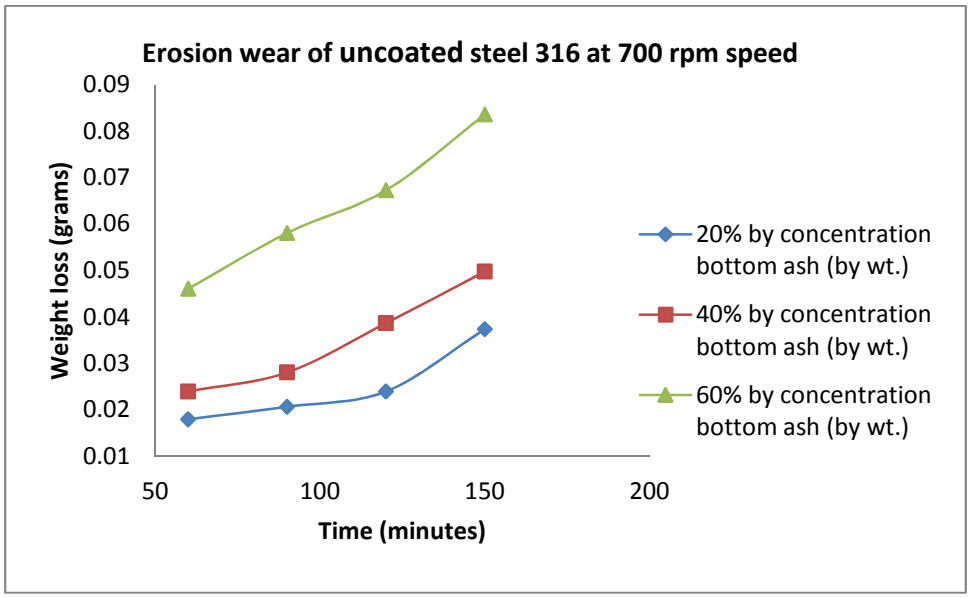

Figure 4.4Erosion wear of uncoated steel 316 at 700 r p m speed

From figure 4.4 seen that at 700r p m speed rate of erosion wear in the terms of weight loss increase 58.89% from 60 minutes to 150 minutes of the operation for handling 20% bottom ash, similarly weight loss increases 42.35% for handling 40% bottom ash and similarly weight loss increases 23.48% for handling 60% bottom ash.

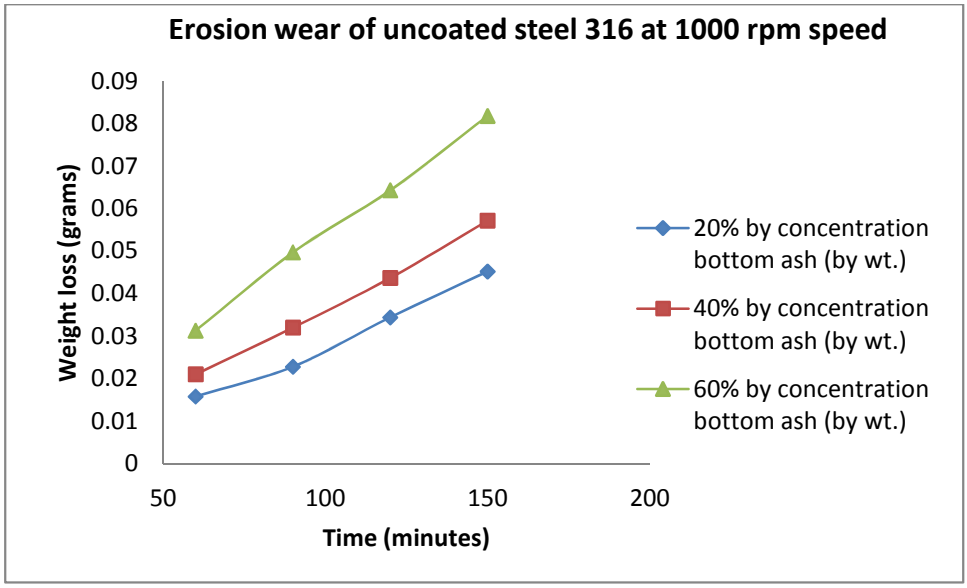

Figure 4.5 Erosion wear of uncoated steel 316 at 1000 r p m speed

From figure 4.5 seen that at 1000r p m speed rate of erosion wear in the terms of weight loss increase 63% from 60 minutes to 150 minutes of the operation for handling 20% bottom ash, similarly weight loss increases 41.79% for handling 40% bottom ash and similarly weight loss increases 40.45% for handling 60% bottom ash.

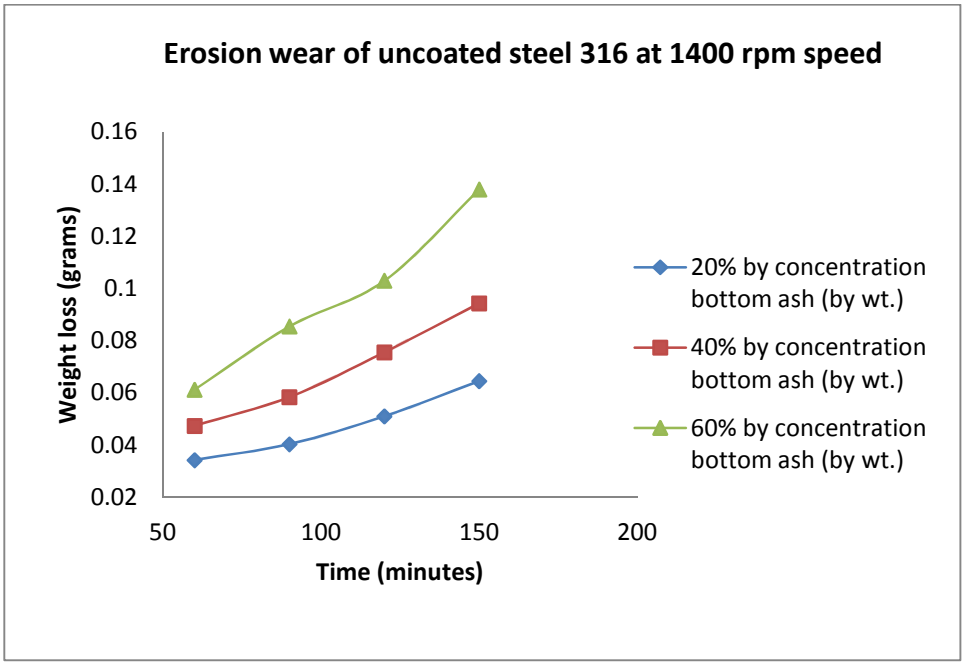

Figure 4.6 Erosion wear of uncoated steel 316 at 1400 r p m speed

From figure 4.6 seen that at 1400r p m speed rate of erosion wear in the terms of weight loss increase 49.43% from 60 minutes to 150 minutes of the operation for handling 20% bottom ash, similarly weight loss increases 34.69% for handling 40% bottom ash and similarly weight loss increases 29.61% for handling 60% bottom ash.

The results reveal that at lower concentration with variation of time of the operation more weight loss occurring as compared to higher concentration.

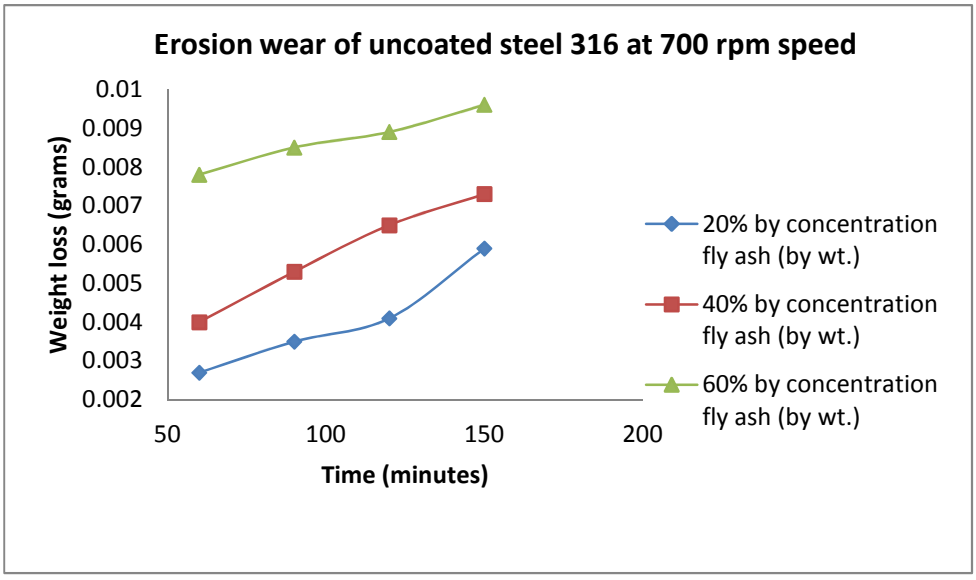

Figure 4.7 Erosion wear of uncoated steel 316 at 700 r p m speed

From figure 4.7 seen that at 700r p m speed rate of erosion wear in the terms of weight loss increase 58.58% from 60 minutes to 150 minutes of the operation for handling 20% fly ash, similarly weight loss increases 43.35% for handling 40% bottom ash and similarly weight loss increases 24.48% for handling 60% fly ash.

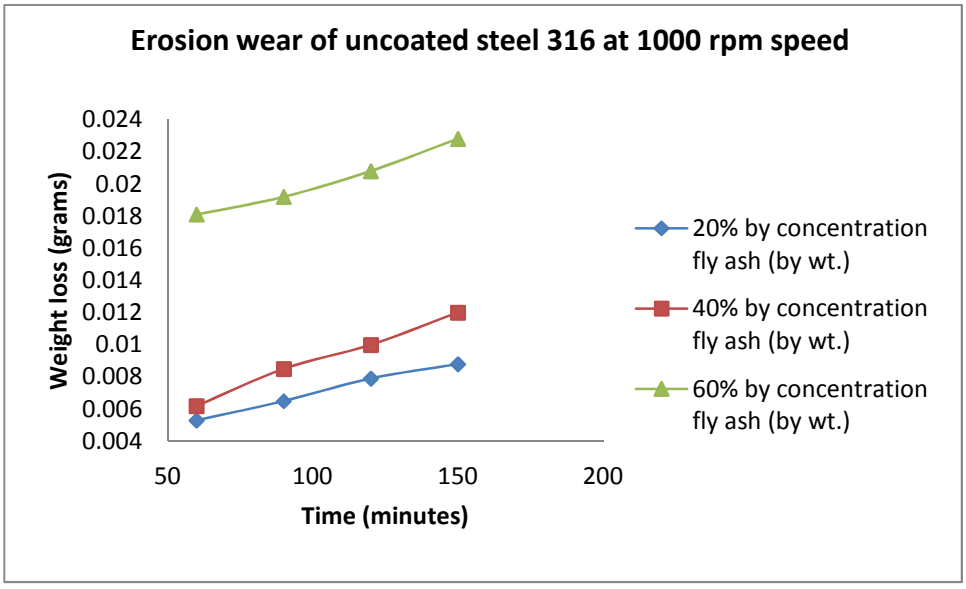

Figure 4.8 Erosion wear of uncoated steel 316 at 1000 r p m speed

From figure 4.8 seen that at 1000r p m speed rate of erosion wear in the terms of weight loss increase 63% from 60 minutes to 150 minutes of the operation for handling 20% fly ash,

similarly weight loss increases 41.56% for handling 40% bottom ash and similarly weight loss increases 40.22% for handling 60% fly ash.

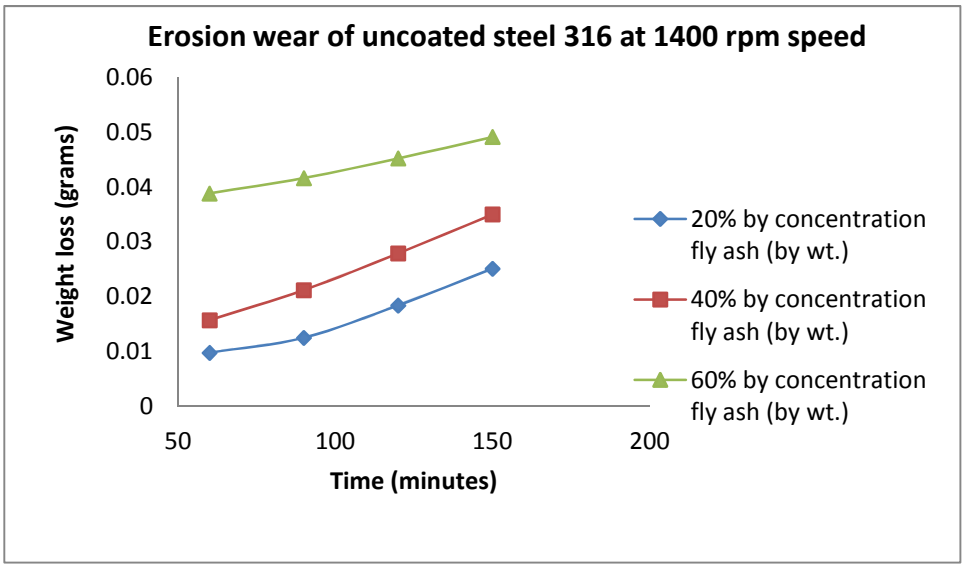

Figure 4.9 Erosion wear of uncoated steel 316 at 1400 r p m speed

From figure 4.9 seen that at 1400r p m speed rate of erosion wear in the terms of weight loss increase 47.43% from 60 minutes to 150 minutes of the operation for handling 20% bottom ash, similarly weight loss increases 32.69% for handling 40% bottom ash and similarly weight loss increases 26.61% for handling 60% fly ash.

Figure 4.4 to 4.9 shows that with the increase of time, speed and concentration of both bottom and fly ash the erosion wear rate increases. As the speed increases the kinetic energy of solid particles of erodent also increases which results in more weight loss. The weight loss of bottom ash as compared to the fly ash is more because the density and size of the bottom ash particles is more. The results reveal that at lower concentration with variation of time of the operation more weight loss occurring as compared to higher concentration.

4.2.2 Scanning Electron Microscope (SEM) of steel 316 without coating

A scanning electron microscope (SEM) is a type of electron microscope that images a sample by scanning it with a high-energy beam of electrons. The electrons interact with the atoms that make up the sample producing signals that contain information about the sample's surface topography, composition, and other properties such as electrical conductivity. The samples of material used for erosion purpose was examined with help of scanning electron microscope with aim to visualize change in microstructure in order to know the mechanism of erosion.

Figure4.10- 4.12 shows the SEM of steel 316 before and after wear at 1400 r p m speed 60% bottom and fly ash.

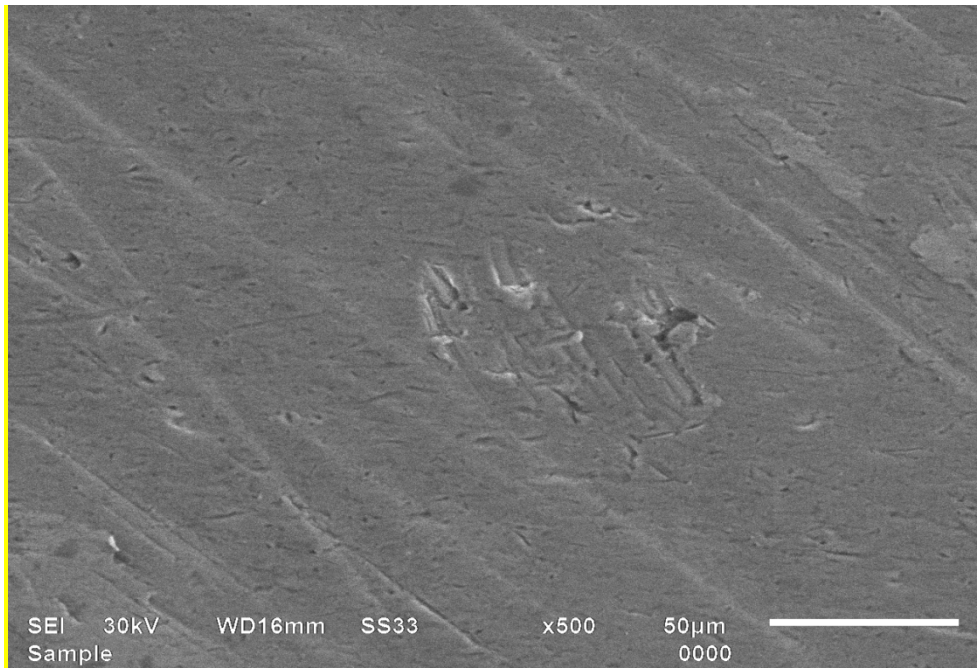

Figure 4.10 SEM of uncoated steel 316 before wear

.

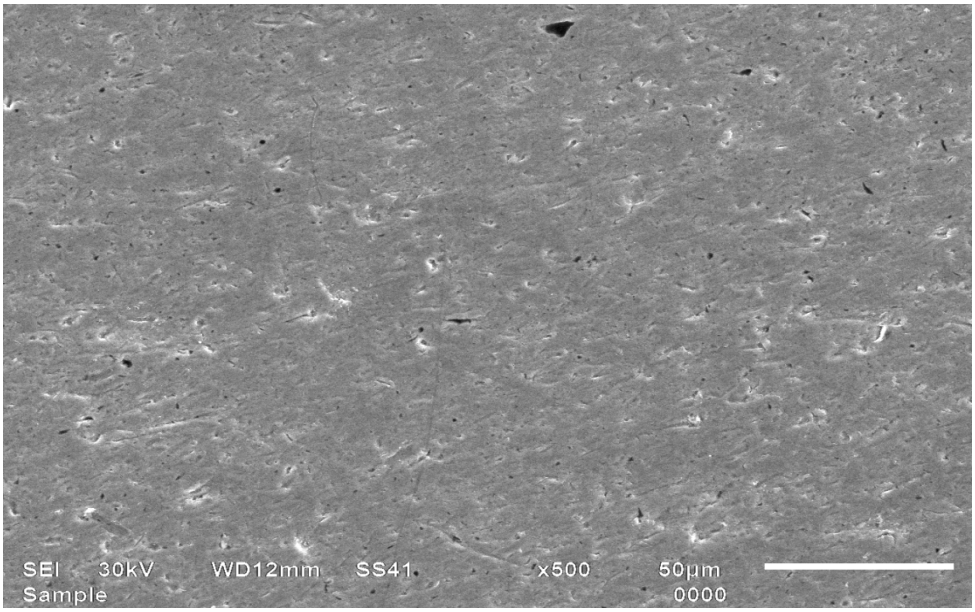

4.11 SEM of uncoated steel 316 after wear at 1400 r p m speed 60% bottom ash

From figure 4.11 observed some creators in the form of black hole along the edges of the surface indicate the loss of material

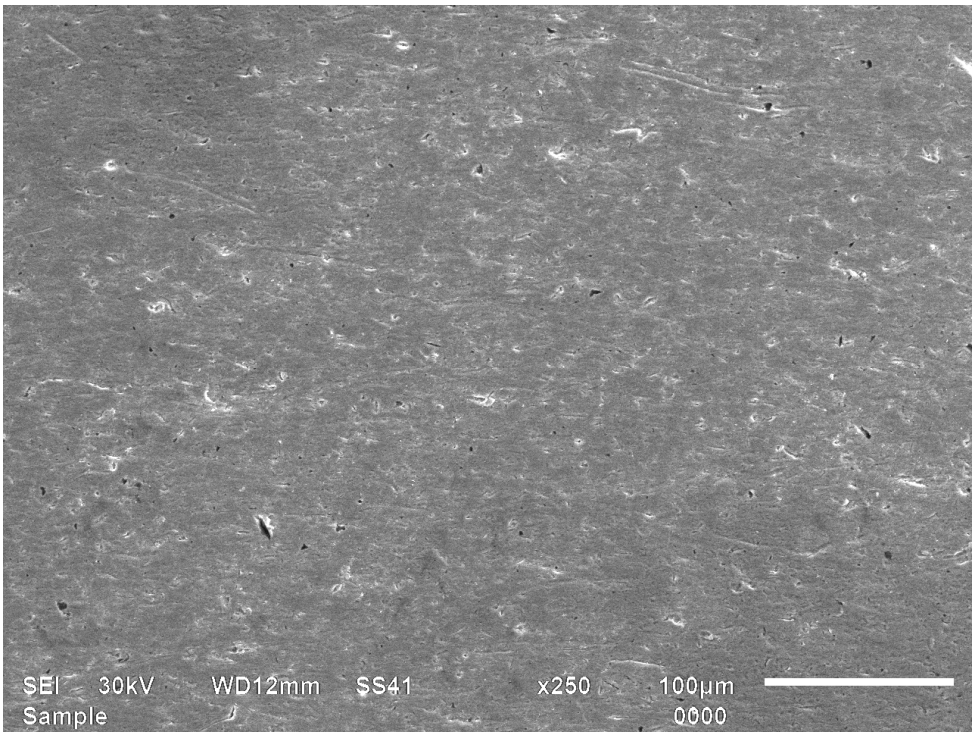

4.12 SEM of uncoated steel 316 after wear at 1400 r p m speed 60% fly ash

Similarly from Figure 4.12 observed some white spots shows the area from where the material has removed.

4.3 EROSION WEAR OF STAINLESS STEEL 420

Steel 420 rectangular specimen runs in pot tester at different speed, time and concentration to find out the erosion of the samples. Weighing machine used for the weight loss measurement before and after the test. Weighing machine has a least count 0.0001mg. Weight loss at different parameters is shown in figure 4.13- 4.18.

4.3.1 Effect of time, speed and concentration

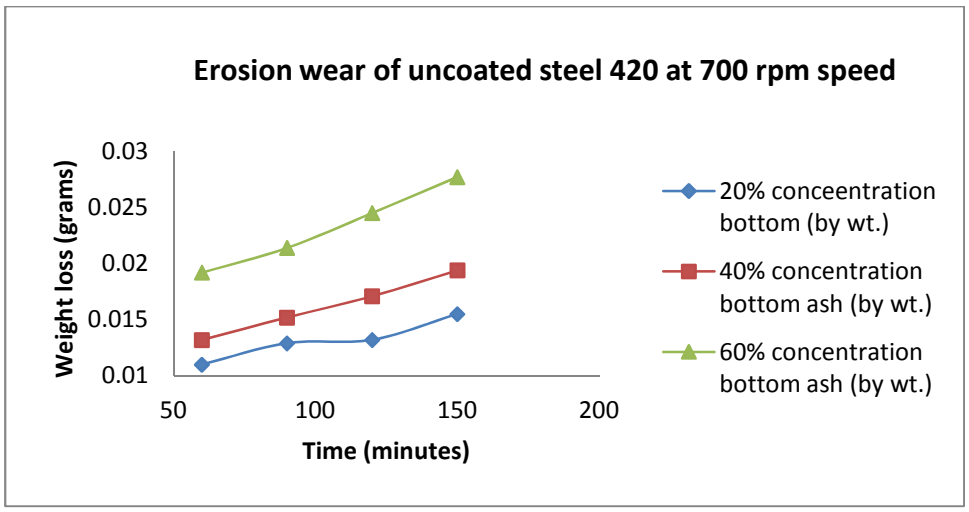

Figure 4.13 Erosion wear of uncoated steel 420 at 700 r p m speed

From figure 4.13 seen that at 700r p m speed rate of erosion wear in the terms of weight loss increase 58.76% from 60 minutes to 150 minutes of the operation for handling 20% bottom ash, similarly weight loss increases 44.25% for handling 40% bottom ash and similarly weight loss increases 24.45% for handling 60% bottom ash.

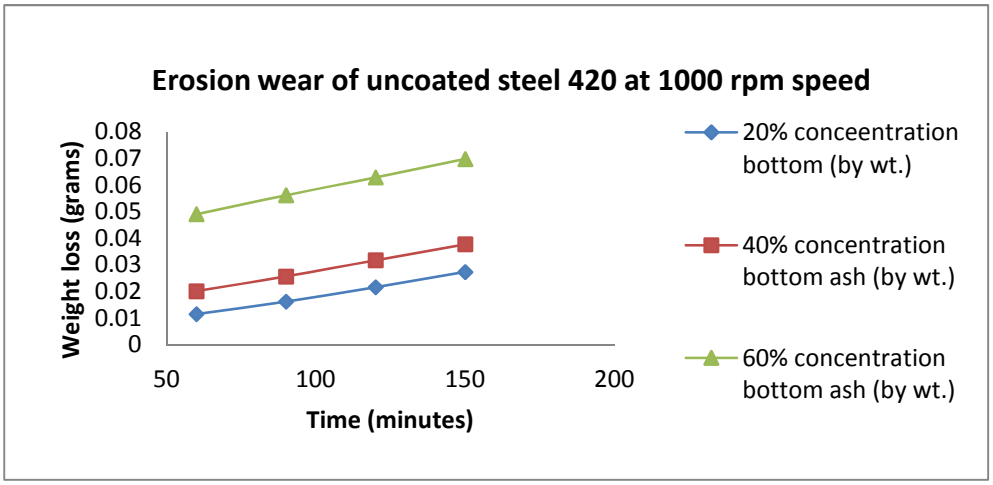

Figure 4.14 Erosion wear of uncoated steel 420 at 1000 r p m speed

From figure 4.14 seen that at 1000r p m speed rate of erosion wear in the terms of weight loss increase 64% from 60 minutes to 150 minutes of the operation for handling 20% bottom ash, similarly weight loss increases 44.53% for handling 40% bottom ash and similarly weight loss increases 40.67% for handling 60% bottom ash.

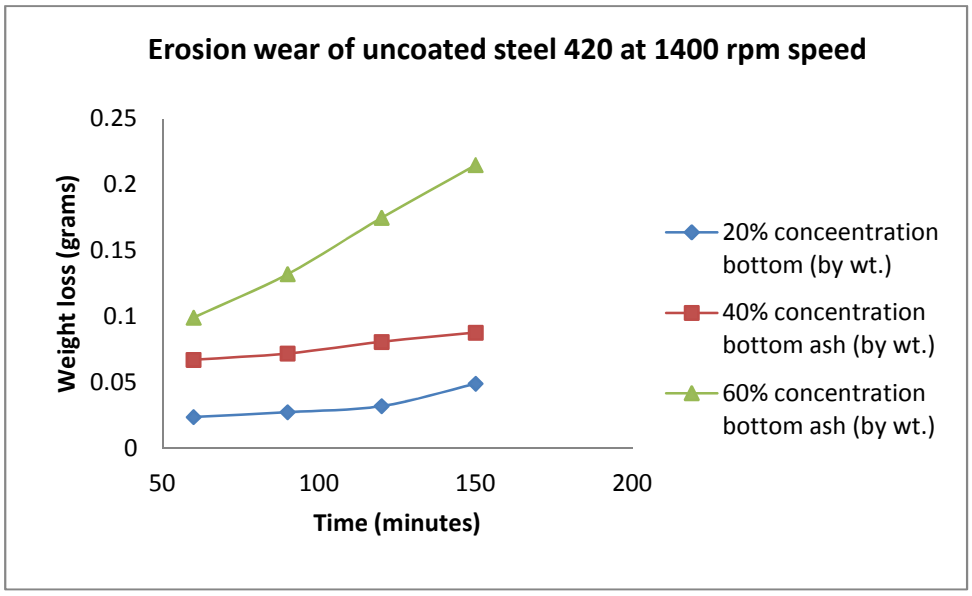

Figure 4.15 Erosion wear of uncoated steel 420 at 1400 r p m speed

From figure 4.15 seen that at 1400r p m speed rate of erosion wear in the terms of weight loss increase 49.43% from 60 minutes to 150 minutes of the operation for handling 20%

bottom ash, similarly weight loss increases 36.67% for handling 40% bottom ash and similarly weight loss increases 29.52% for handling 60% bottom ash.

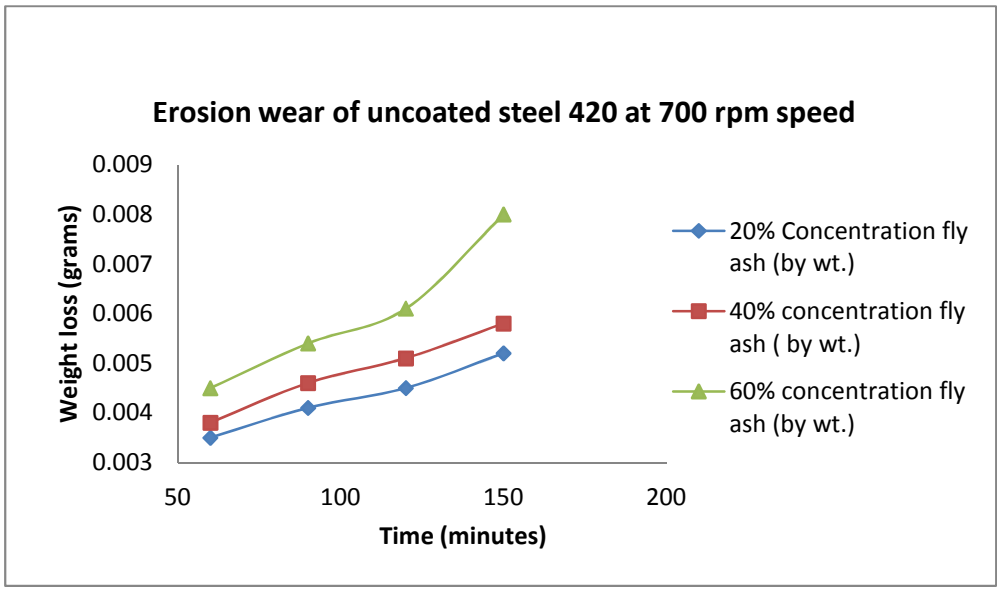

Figure 4.16 Erosion wear of uncoated steel 420 at 700 r p m speed

From figure 4.16 seen that at 700r p m speed rate of erosion wear in the terms of weight loss increase 56.58% from 60 minutes to 150 minutes of the operation for handling 20% fly ash, similarly weight loss increases 41.59% for handling 40% bottom ash and similarly weight loss increases 27.31% for handling 60% fly ash.

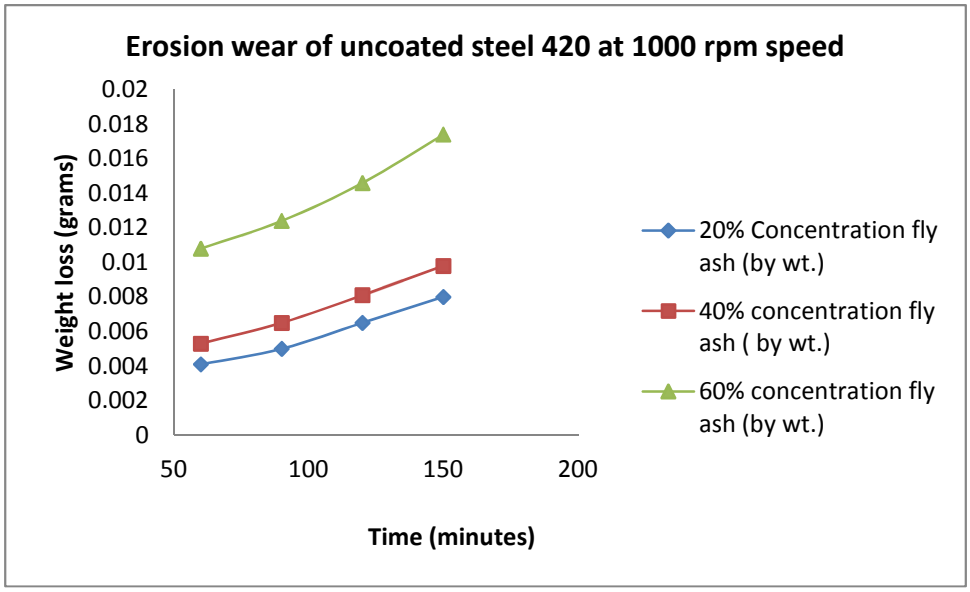

Figure 4.17 Erosion wear of uncoated steel 420 at 1000 r p m speed

From figure 4.17 seen that at 1000r p m speed rate of erosion wear in the terms of weight loss increase 62% from 60 minutes to 150 minutes of the operation for handling 20% fly ash, similarly weight loss increases 41.28% for handling 40% bottom ash and similarly weight loss increases 38.47% for handling 60% fly ash.

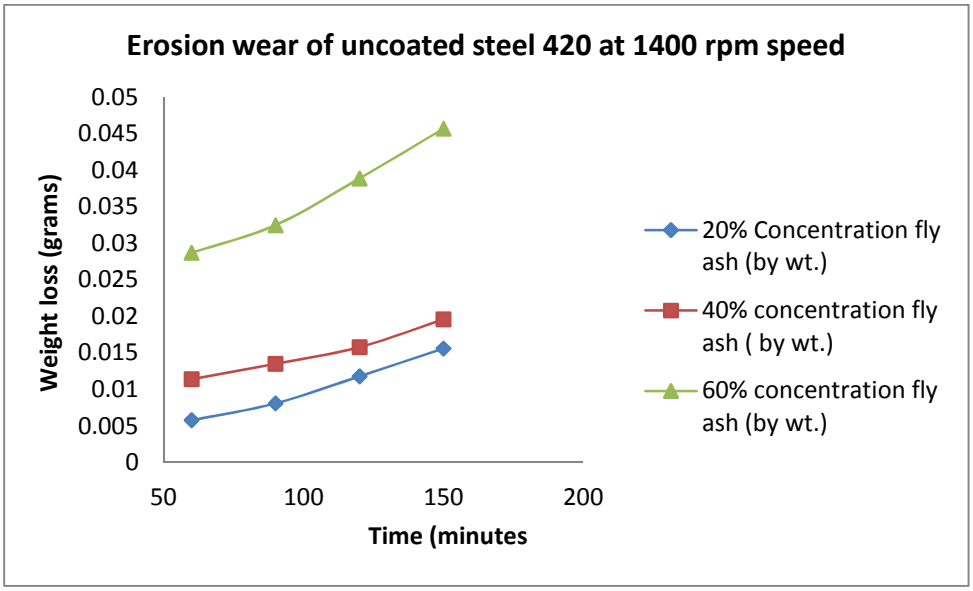

Figure 4.18 Erosion wear of uncoated steel 420 at 1400 r p m speed

From figure 4.18 seen that at 1400r p m speed rate of erosion wear in the terms of weight loss increase 50.18% from 60 minutes to 150 minutes of the operation for handling 20% fly ash, similarly weight loss increases 36.79% for handling 40% bottom ash and similarly weight loss increases 29.64% for handling 60% fly ash.

Figure 4.13 to 4.18 shows that with the increase of time, speed and concentration of both bottom and fly ash the erosion wear rate increases. As the speed increases the kinetic energy of solid particles of erodent also increases which results in more weight loss. The weight loss of bottom ash as compared to the fly ash is more because the density and size of the bottom ash particles is more. The results reveal that at lower concentration with variation of time of the operation more weight loss occurring as compared to higher concentration

4.3.2 Scanning Electron Microscope (SEM) of steel 420 without coating

Figure 4.19-4.21 shows the SEM of steel 420 at higher magnification before and after wear.

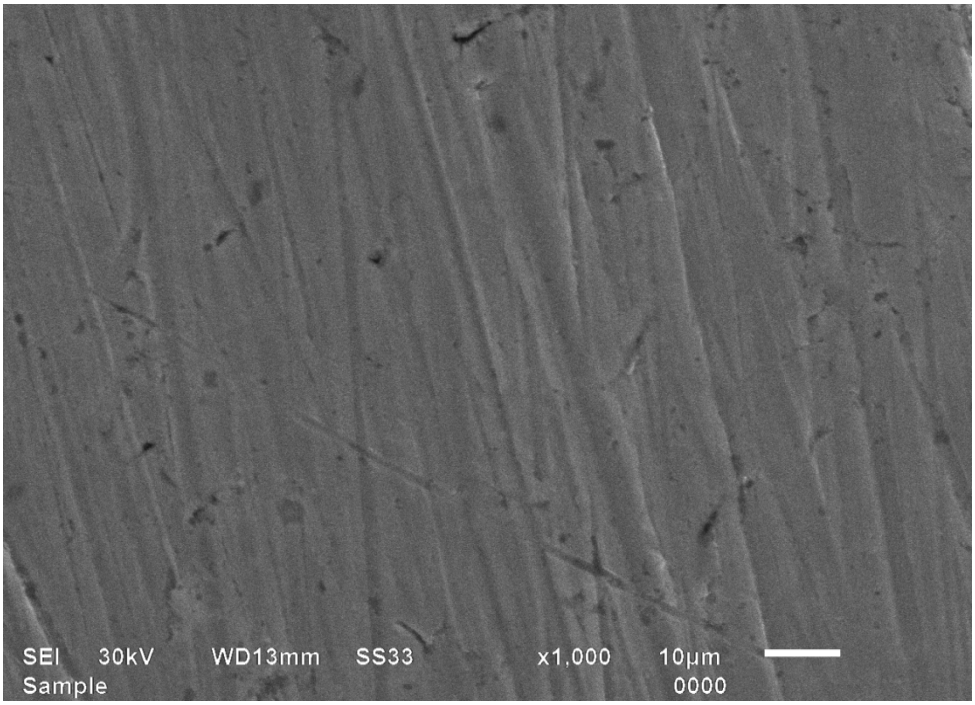

Figure 4.19 SEM of uncoated steel 420 before wear

From figure 4.19 observed that before wear structure of steel 420 is clearly visible.

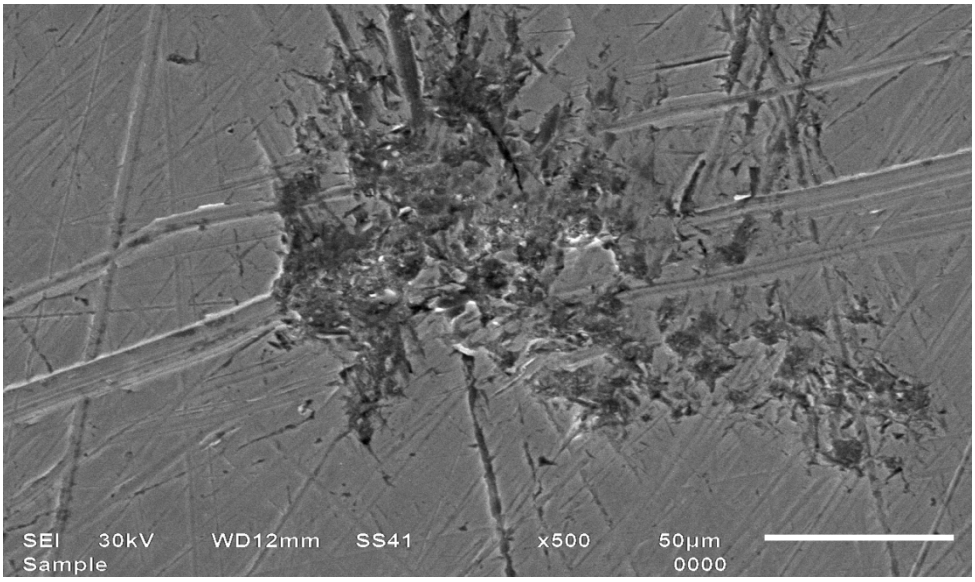

4.20 SEM of uncoated steel 316 after wear at 1400 r p m speed 60% bottom ash

From Figure 4.20 observed that at 1400 r p m speed bottom ash sticks along the edges of the steel, indicates removal of material from the edges. Craters come in picture in the micrographs due to more erosion by impact of the particles.

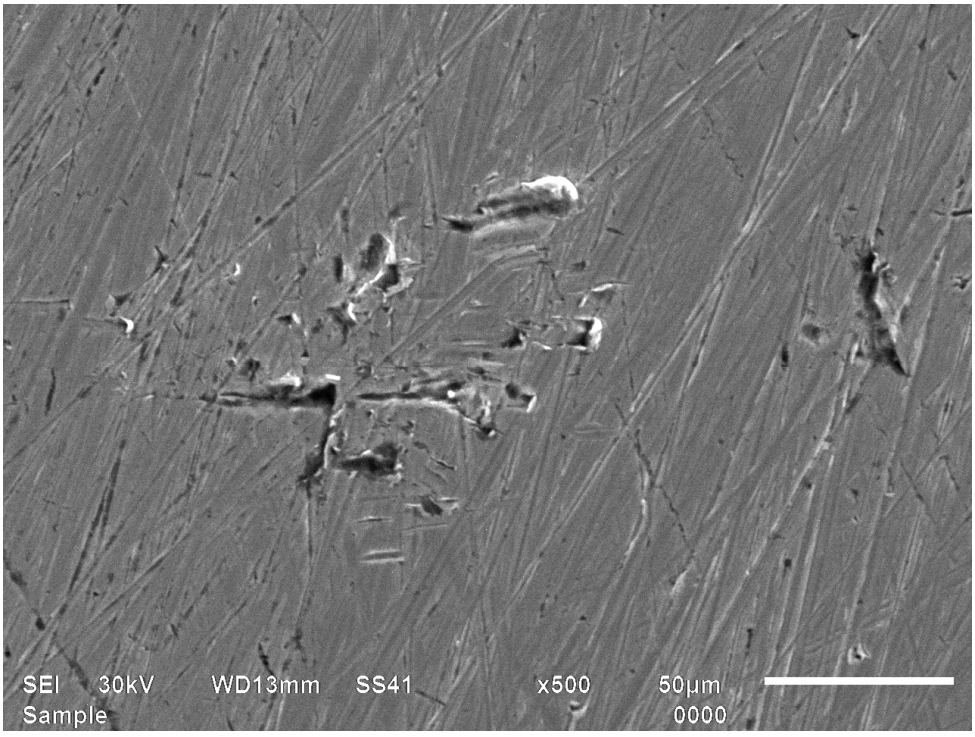

4.21 SEM of uncoated steel 316 after wear at 1400 r p m speed 60% fly ash

Similarly from figure 4.21 observed that less fly ash particles stick along the steel edges which leads to less wear rate. It is also observed that less material craters as compare to bottom ash.

4.4 COATING TECHNIQUE FOR THE PUMP MATERIALS (ELECTROPLATING)

Electroplating is a plating process in which metal ions in a solution are moved by an electric field to coat an electrode. The process uses electrical current to reduce cations of a desired material from a solution and coat a conductive object with a thin layer of the material, such as a metal.

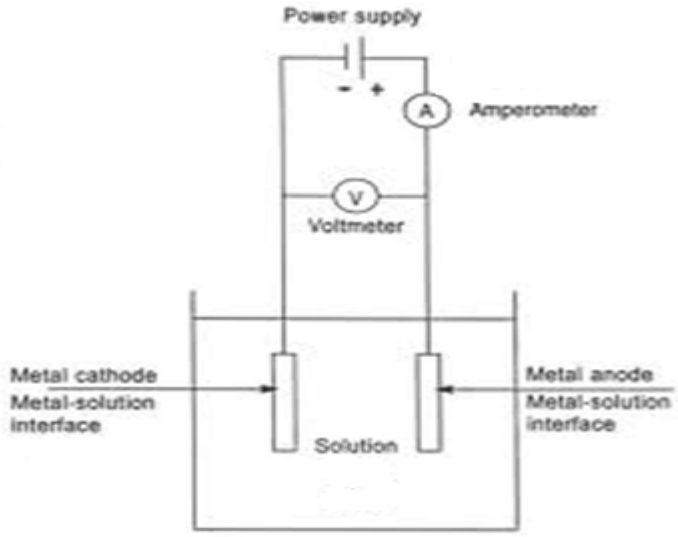

Figure 4.22 Electroplating technique

In this process, chromium plate is placed at anode and steel 316 and steel 420 samples at cathode in a bath of chromium sulphate one by one. Chromic acid as sold is not truly chromic acid it actually chromium trioxide or chromium anhydride and is not an acid until it dissolved in water. Chromium trioxide dissolved in water and form chromic acid. Chromium is oxidized at the anode to Cr^{2+} by losing two electrons. The Cr^{2+} associates with the anion SO_4^{2-} in the solution to form. At the cathode, the Cr^{2+} is reduced to metallic chromium by gaining two electrons. The result is the effective transfer of chromium from the anode source to a steel 316 and steel 420 plates covering the cathode.

Figure 4.23- 4.28 show the wear rate of coated steel 316 and steel 420 at 700, 1000, 1400 r p m speed , with bottom ash concentration 20, 40, 60% by weight .

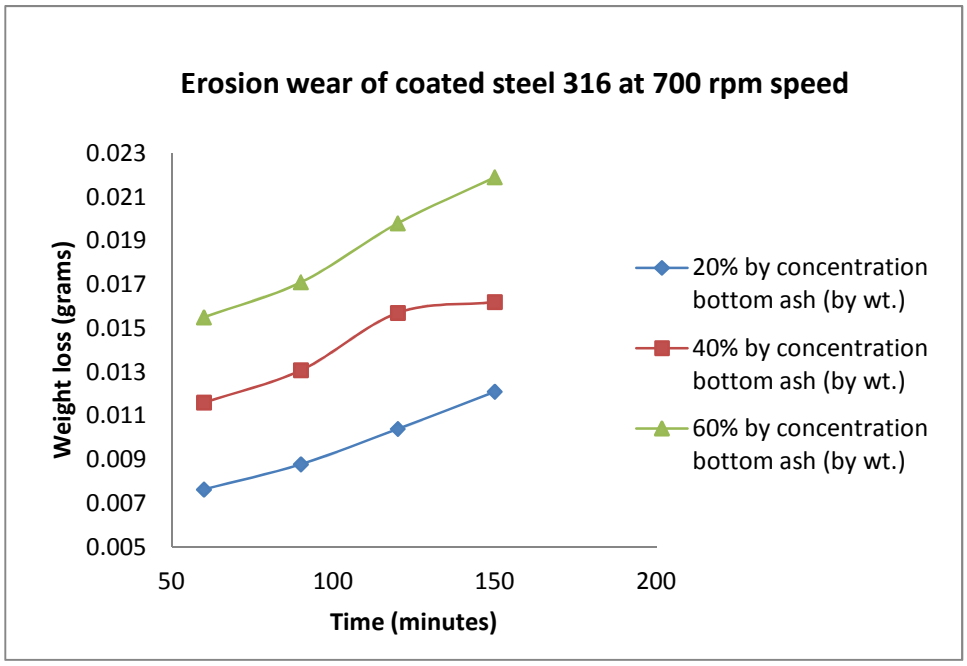

Figure 4.23 Erosion wear of coated steel 316 at 700 r p m speed

From figure 4.23 noted that at 700r p m speed rate of erosion wear in the terms of weight loss increase 45.10% from 60 minutes to 150 minutes of the operation for handling 20% bottom ash, similarly weight loss increases 37.9% for handling 40% bottom ash and similarly weight loss increases 27.5% for handling 60% bottom ash.

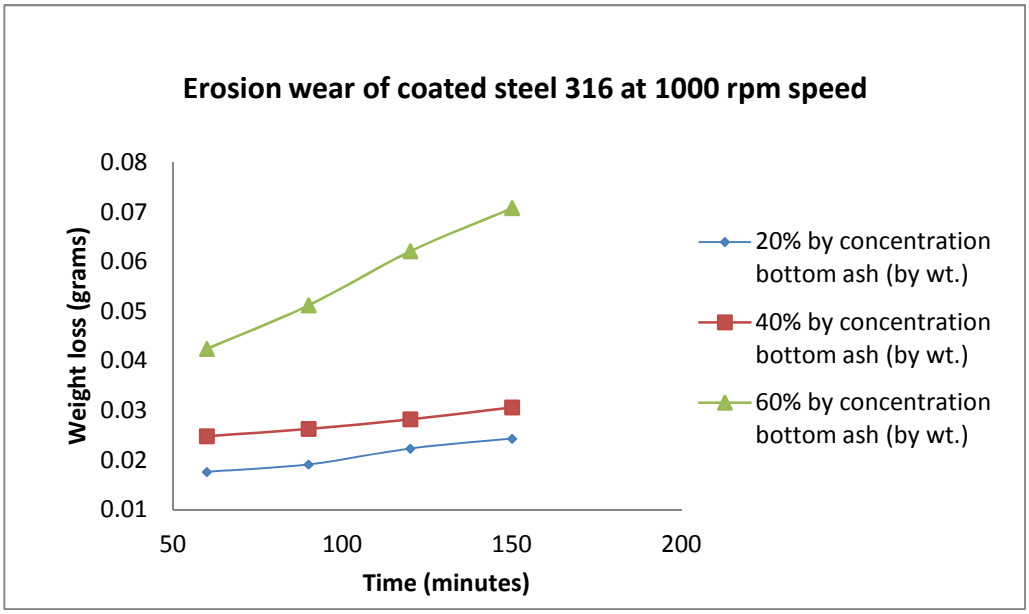

Figure 4.24 Erosion wear of coated steel 316 at 1000 r p m speed

From figure 4.24 noted that at 1000r p m speed rate of erosion wear in the terms of weight loss increase 31.56% from 60 minutes to 150 minutes of the operation for handling 20% bottom ash coated steel 316, similarly weight loss increases 26.17% for handling 40% bottom ash and similarly weight loss increases 14.44% for handling 60% bottom ash.

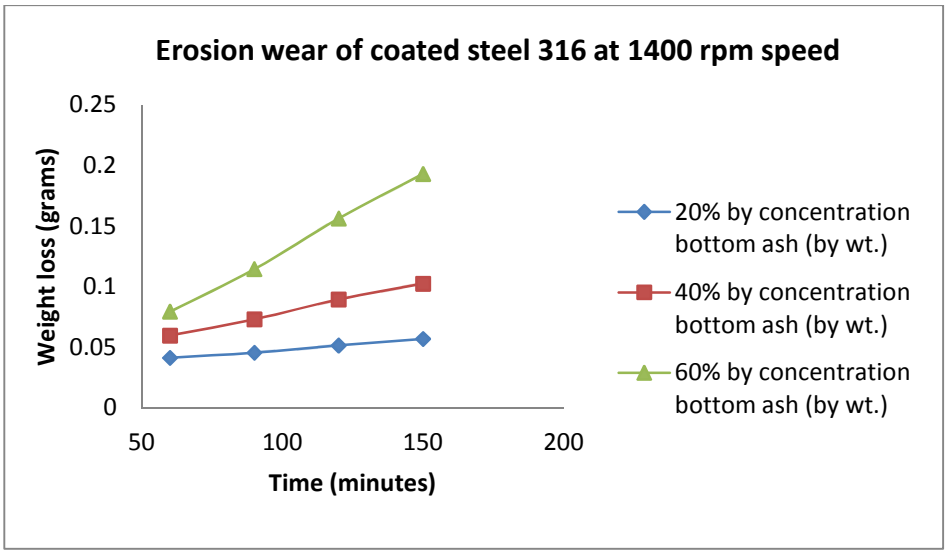

Figure 4.25 Erosion wear of coated steel 316 at 1400 r p m speed

Figure 4.26- 4.28 observed that erosion wear of coated steel 420 increases with time of operation 60 to 150 minutes and between 120 to 150 minute rate of erosion wear increases very slowly as compared to time of operation between 60 to 120 minutes. It is also observed that rate of erosion wear increases with the changing the concentration of bottom ash and with the changing the speed.

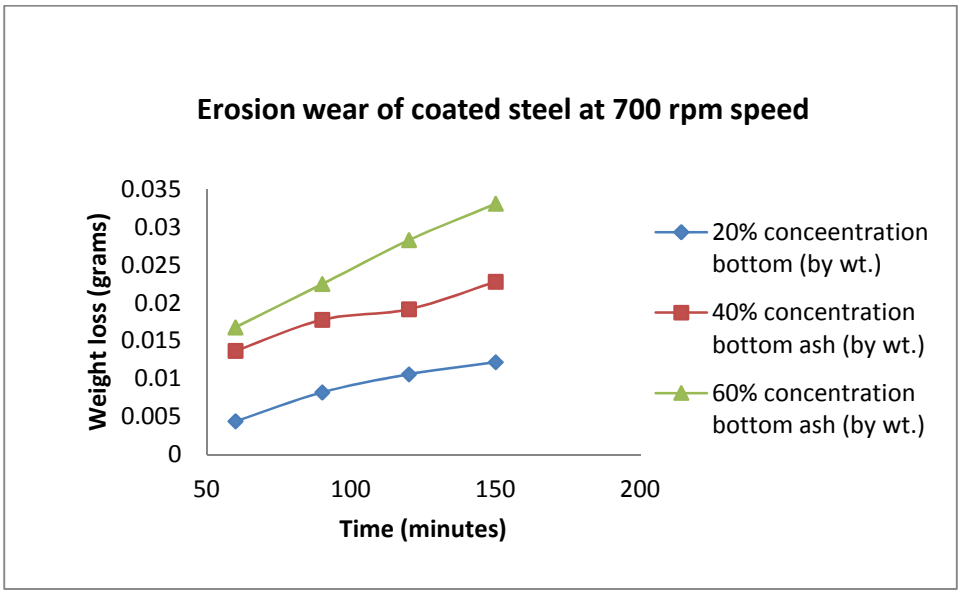

Figure 4.26 Erosion wear of coated steel 420 at 700 r p m speed

From figure 4.26 seen that at 700r p m speed rate of erosion wear in the terms of weight loss increase 66.24% from 60 minutes to 150 minutes of the operation for handling 20% bottom ash, similarly weight loss increases 61.7% for handling 40% bottom ash and similarly weight loss increases 59% for handling 60% bottom ash.

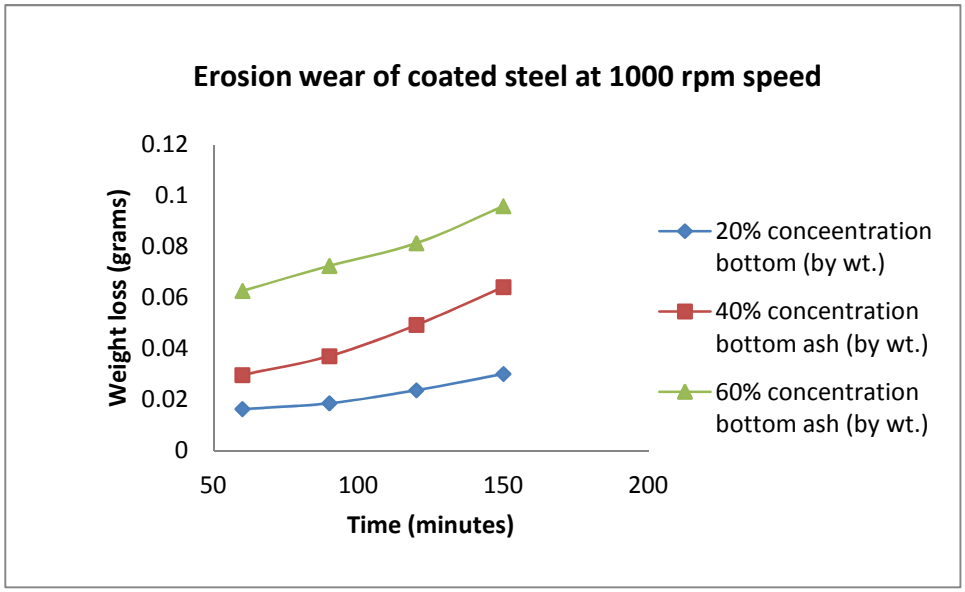

Figure 4.27 Erosion wear of coated steel 420 at 1000 r p m speed

From figure 4.27 observed that at 1000r p m speed rate of erosion wear in the terms of weight loss increase 53% from 60 minutes to 150 minutes of the operation for handling 20% bottom ash, similarly weight loss increases 49% for handling 40% bottom ash and similarly weight loss increases 42% for handling 60% bottom ash.

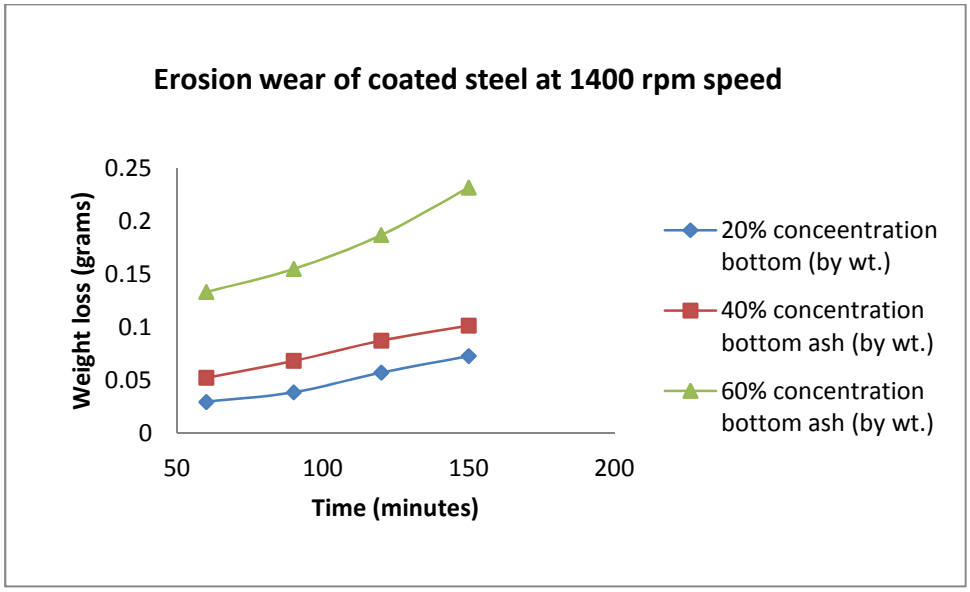

Figure 4.28 Erosion wear of coated steel 420 at 1400 r p m speed

From figure 4.28 noted that at 1400r p m speed rate of erosion wear in the terms of weight loss increase 47% from 60 minutes to 150 minutes of the operation for handling 20% bottom ash, similarly weight loss increases 33% for handling 40% bottom ash and similarly weight loss increases 40% for handling 60% bottom ash.

The results reveal that at lower concentration with variation of time of the operation more weight loss occurring as compared to higher concentration

4.4.1 SEM of coated steel 316 and 420

From figure 4.29 and 4.32 shows the SEM with coating on the surface of steel 316 and steel 420 before and after wear.

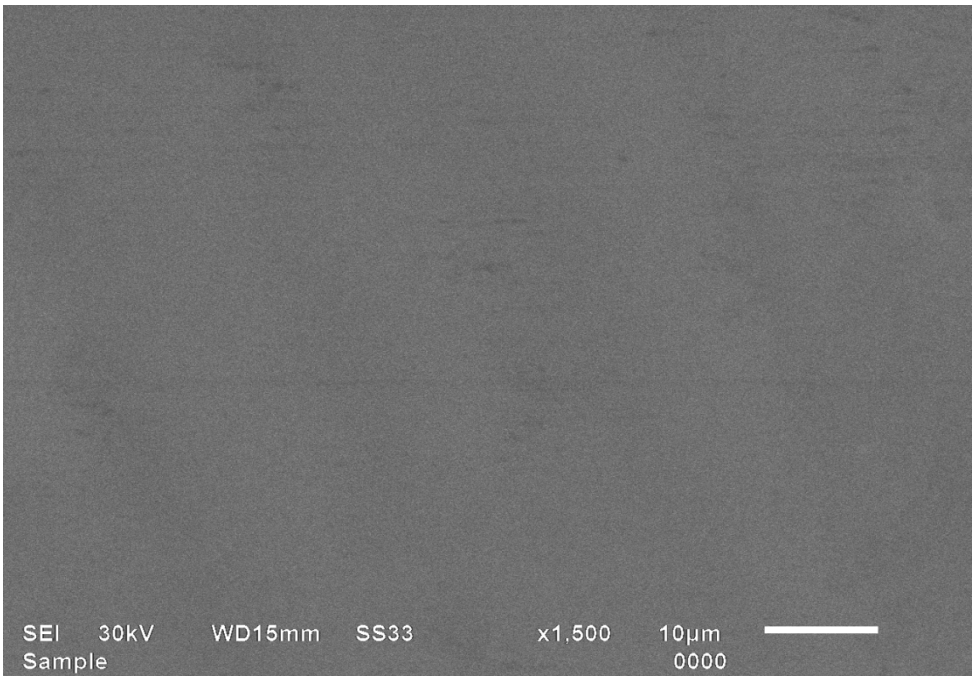

Figure 4.29 SEM of coated steel 316 before wear

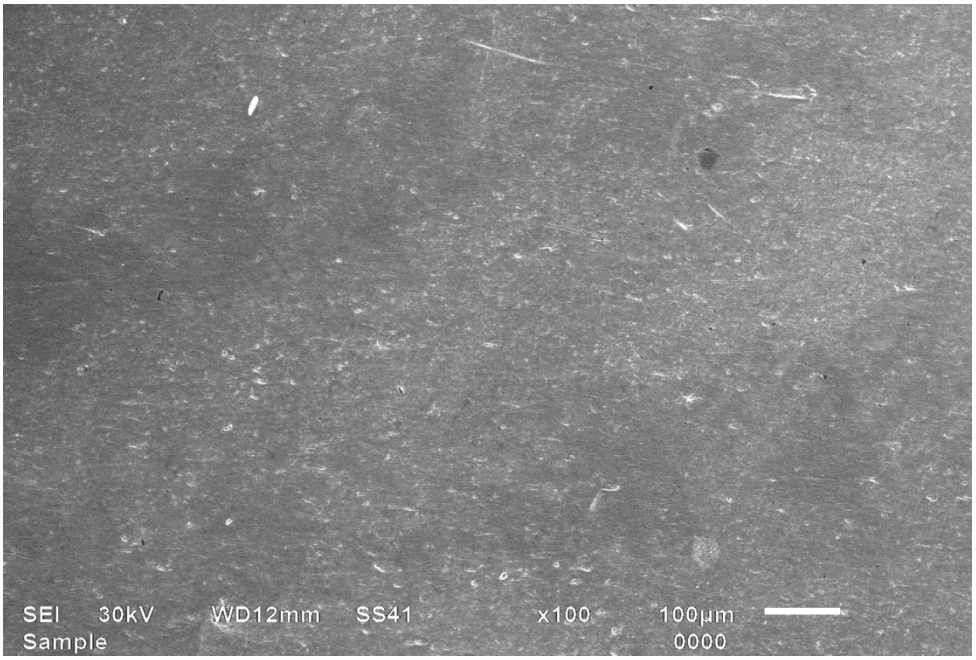

Figure 4.30 SEM of coated steel 316 after wear

Figure 4.30 shows small indication of some white spots on steel 316 coated surfaces after wear. It indicates removal of material from the surface due to the attack of bottom ash.

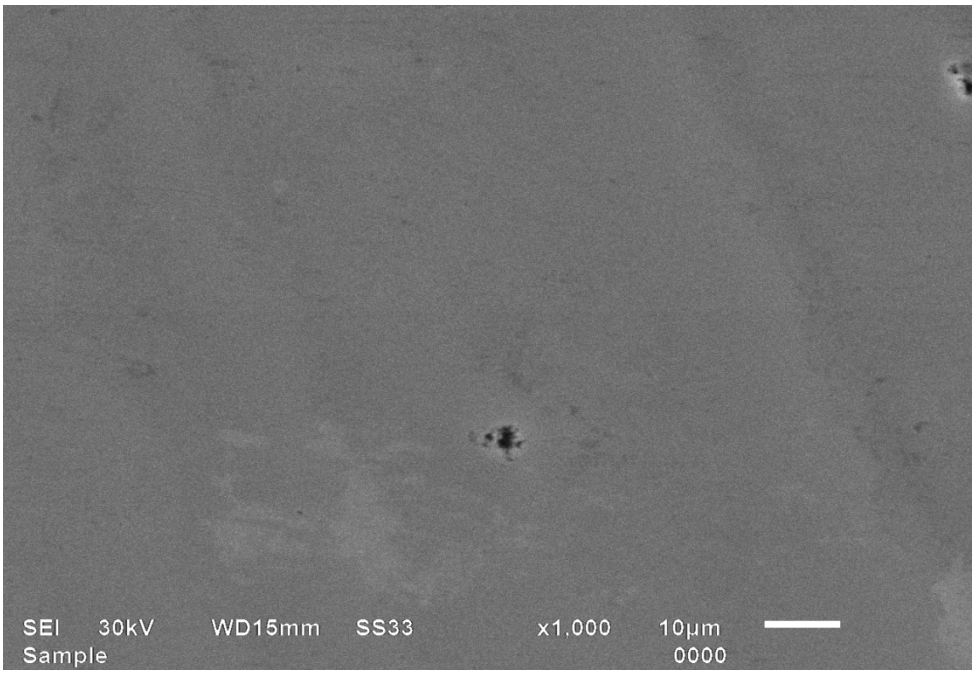

Figure 4.31 SEM of coated steel 420 before wear

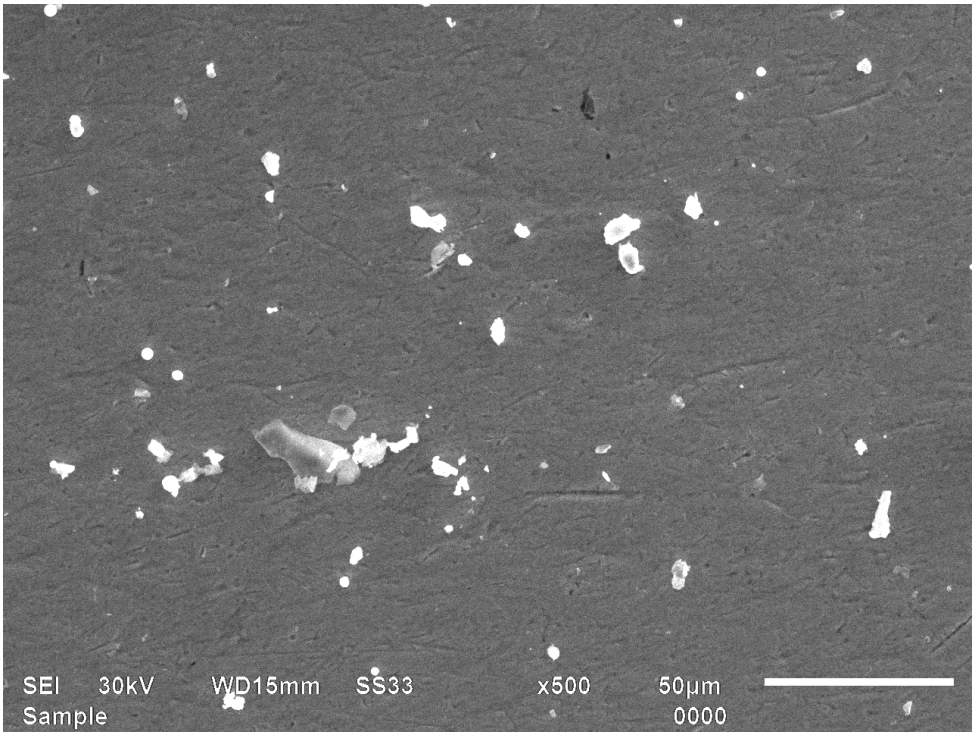

Figure 4.32 SEM of coated steel 420 after wear

Figure 4.32 shows small indication of some white spots on steel 420 coated surfaces after wear. It indicates removal of material from the surface due to the attack of bottom ash. It is observed that coated steel 316 and 420 show better erosion resistance as compare to uncoated steel 316 and 420.

CHAPTER 5

EVALUATION OF EROSION WEAR USING CFD

5.1 INTRODUCTION TO CFD

Computational fluid dynamics (CFD) is one of the branches of fluid mechanics that uses numerical methods and algorithms to solve and analyze problems that involve fluid flows. CFD has become an indispensable tool in the design, development, evaluation and refinement of new industrial equipment and processes. The use of CFD reduces the development cost of new products and cuts the time to market of these products.

Computational Fluid Dynamics (CFD) has become an integral part of the engineering design cycle. Whether it is used to design industrial mixing tanks, aerospace components, or used to simulate transient flow phenomenon in pumps and turbines.CFD analyses reduce development time and increase the reliability of prototype designs. CFD simulations can be used to model fluid flows over a wide range of physical scales.

5.2 CFD METHODOLOGY

In order to obtain better design in CFD, following procedure is applied so that fluid flow can easily be modelled.

5.2.1 Initial design

Initial design of the model is a planning decision and the geometry is generated depending on these initial design considerations, using either CFD modelling tools or other Design tools.

5.2.2 Geometry generation

The first task to accomplish in a numerical flow simulation is the definition of the geometry, followed by the grid generation. This step is the most important step for the study of an isolated impeller assuming an axis symmetric flow simplifies the domain to a single blade passage.

The geometry of design needs to be created from the initial design. Any modelling software can be used for modelling and then shifted to other simulation software for analysis purposes.

5.2.3 Mesh generation

Mesh generation (Gridding) is the process of subdividing a region to be modelled into a set of small control volumes. Associated with each control volume there will be one or more values of the dependent flow variables (e.g., velocity, pressure, temperature, etc.) Usually these represent some type of locally averaged values. Meshing is a method to define and break up the model into small elements. In general, a finite element model is defined by a mesh network, which is made up of the geometric arrangement of elements and nodes. Nodes represent points at which features such as displacements are calculated. Elements are bounded by sets of nodes, and define localized mass and stiffness properties of the model. The traditional method of mesh generation is block-structure (multi-block) mesh generation. The block-structure approach is simple and efficient technique of mesh generation.

5.2.4 Pre-processing

5.2.4.1 Boundary condition

The first step in Pre-processing is setting up the boundary conditions. Boundary condition will be different for each type of problem. In Cartesian and cylindrical-polar coordinates, the location of boundary features (inlets, outlets, blockages, etc) can be linked to named 'objects' defined during the grid-generation procedure. This obviates the need to enter the coordinates twice: once when defining the grid, and again when specifying boundary conditions. In low speed and incompressible flows, disturbances introduced at an out flow boundary can have an effect on the entire computational region. As a general rule, a physically meaningful boundary condition, such as a specified pressure condition, should be used at out flow boundaries whenever possible. Generally, a pressure condition cannot be used at a boundary where velocities are also specified, because velocities are influenced by pressure gradients. The inlet condition for velocity and temperature can be specified using profile of grid. The turbulent kinetic energy (k) and its dissipations rate can be calculated from the value of turbulence intensity specified in the inlet.

5.2.4.2 Multiphase flow

Multiphase flow is a flow in which more than one fluid is present. In general, the fluids consist of different chemical species, e.g., air-water. In some applications, they may represent different thermodynamic phases of the same species, e.g., steam-water.

5.2.4.3Basic erosion model

a) Model of Finnie

The wear of a wall due to the erosive effect of particle impacts is a complex function of particle impact, particle and wall properties. For nearly all metals, erosion is found to vary with impact angle and velocity according to the relationship

$$E = k\, V_P^n\, f(\gamma)$$

Where

E = dimensionless mass

V_p= particle impact velocity

$f(\gamma)$= a dimensionless function of the impact angle

The impact angle is the angle in radians between the approaching particle track and the wall. The value of the exponent is generally in the range 2.3 to 2.5 for metals. Finnie's model of erosive wear relates the rate of wear to the rate of kinetic energy of impact of particles on the surface, using n = 2,

$f(\gamma) = 1/3 \cos^2\gamma$ if $\tan\lambda > 1/3$

$f(\gamma) = \sin(2\lambda) - 3sin^2\gamma$ if $\tan\lambda \leq 1/3$

b) Model of Tabakoff and Grant

In the erosion model of Tabakoff and Grant, the erosion rate E is determined from the following relation:

$$E = k_1 f(\gamma) V_P^2 cos^2\gamma [1 - R_T^2] + f(V_{PN})$$

$$f(\gamma) = \left[1 + k_2 k_{12} \, sin\left(\gamma \frac{\pi/2}{\gamma_0}\right)\right]^2$$

$$R_T = 1 - k_4 V_P sin\gamma$$

$$f(V_{PN}) = k_3 (V_P sin\gamma)^4$$

$$k_2 = \begin{cases} 1.0 \; if \gamma \leq 2\gamma_0 \\ 0.0 \; if \; \gamma > 2\gamma_0 \end{cases}$$

Where

E= Dimensionless mass (mass of eroded wall material divided by the mass of particle)

V_p= Particle impact velocity

γ = Impact angle in radians between the approaching particle track and the wall,

γ_0=Angle of maximum erosion,

k_1, k_2, k_3, k_4, k_{12} are model constants which depend upon particle perwall material combination.

The erosion rate calculated as:

Erosion Rate (grams) =Erosion rate density × surface area× time

Erosion rate (grams) = $\frac{kg}{s.m^2} \times m^2 \times s \times 1000$

Restitution Coefficient

Restitution behaviour is a measure of the momentum lost by the particle at impact as such and it corresponds to the work done on the target surface, which, in turn, is a measure of the extent of erosion suffered by the material of the target surface. The velocity coefficients of restitution depend upon the hardness of the target material, the density of the particle and the impact velocity.

5.2.4.4Solver

Navier-Stokes Equation

The set of equations which describe the processes of momentum, heat and mass transfer are known as the Navier-Stokes equations. Equations processes, such as combustion, can also be solved in conjunction with the Navier-Stokes equations. Often, an approximating model is used to derive these additional equations, turbulence models being a particularly important example. The Navier-Stokes equations, named after Claude-Louis Navier and George Gabriel Stokes, describe the motion of fluid substances such as liquids and gases. These equations establish that changes in momentum in infinitesimal volumes of fluid are simply the sum of dissipative viscous forces (similar to friction), changes in pressure, gravity, and other forces acting inside the fluid: an application of Newton's second law.

The Navier-Stokes equations are differential equations which, unlike algebraic equations, do not explicitly establish a relation among the variables of interest (e.g. velocity and pressure). Rather, they establish relations among the rates of change. For example, the Navier-Stokes equations for simple case of an ideal fluid (inviscid) can state that acceleration (the rate of change of velocity) is proportional to the gradient (a type of multivariate derivative) of pressure.

A two dimensional, laminar incompressible flow with constant viscosity is described by:

X-Momentum $$\rho\frac{\partial u}{\partial t}+\rho u\frac{\partial u}{\partial x}+\rho v\frac{\partial u}{\partial y}=\mu\left(\frac{\partial^2 u}{\partial x^2}+\frac{\partial^2 u}{\partial y^2}\right)-\frac{\partial \rho}{\partial x}$$

Y-Momentum $$\rho\frac{\partial v}{\partial t}+\rho u\frac{\partial v}{\partial x}+\rho v\frac{\partial v}{\partial y}=\mu\left(\frac{\partial^2 v}{\partial x^2}+\frac{\partial^2 v}{\partial y^2}\right)-\frac{\partial \rho}{\partial x}$$

And continuity $$\frac{\partial u}{\partial x}+\frac{\partial v}{\partial y}=0$$

Where

u = Component of Velocity in x-direction

v = Component of Velocity in y-direction

μ = Viscosity of Fluid

ρ = Density of fluid

Post-Processing

Post-processing provides the CFD professional with easy-to-use powerful result visualization features for structured, unstructured, and hybrid grids. It provides an in depth view of data with visualization tools such as cutting planes, contouring, streamlines, line plots, data probes and animation. Animations can be created by saving CFD solutions with or without skipping certain number of time steps and playing the saved frames in a continuous sequence. Animations are important tools to study time dependent developments of vertical /turbulent structures and their interactions.

5.3 PREPRATION OF CAD MODEL AND MESH GENEATION

The next step after taking the dimensions are preparing the cad model. The cad model was modeled by using Pro-engineering software. For modeling of impellor the points obtained on graph were then plotted in the software following which a curve with a suitable radius was fitted through the points to get the smooth surface. In case of casing each sector was then drawn over a base circle in the software. The cross-section was drawn by connecting the points with Nerbs. Once the cross-section of each sector was made, the casing was constructed with the bottom up approach by creating faces and volumes. Similarly modeling was done of other parts of the pump and they were later moved to their respective places for assembly purpose. The cad model of casing, impellor and inlet passage is shown on figure 5.1.

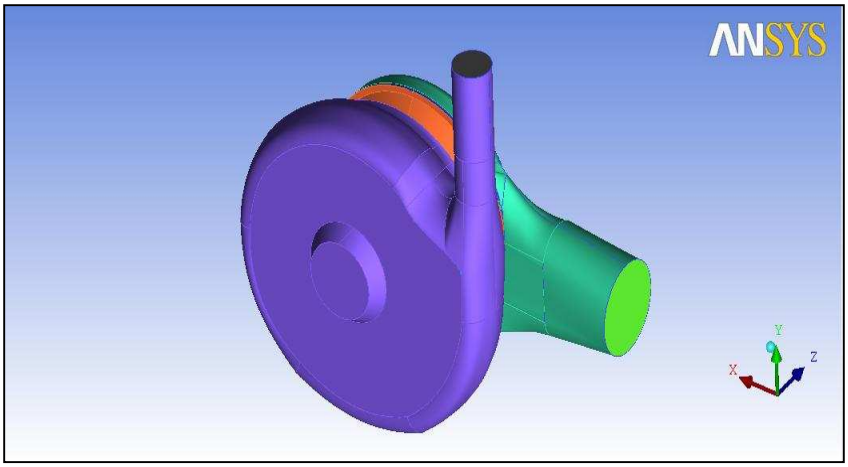

Figure 5.1 assembled view of centrifugal pump

The first step after modeling the pump components is discretizing it into smaller elements. The model is discretized so that the affect of external or internal forces acting on a body can be captured at any point on the body. This process of Discretization is called meshing. The larger the number of these elements, finer will be the mesh which will give accurate result. But a large number of elements or a fine mesh needs greater computational capabilities and time. To optimize the meshing, a finer mesh is used at points where the forces have maximum impact and a coarser mesh is used at other locations. For meshing, the model was taken to a commercially available ANSYS ICEM 13.0 was used. It provides a large variety of tools for meshing. The tetrahedral type of elements was used for the Discretization of all the three components of the centrifugal pump. The meshed photographic view of pump is shown in figure 5.2.

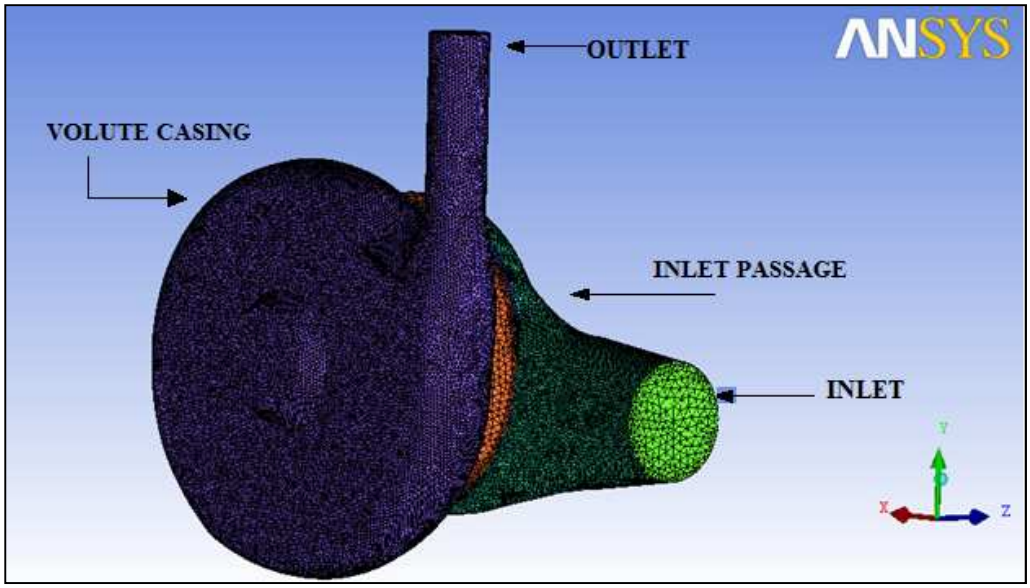

Figure 5.2 Meshed model of centrifugal pump

The information about no. of elements is given in table 5.1

Table 5.1 Number of elements

Part name	No. of elements
Inlet passage	180988
Casing	185360
Impellor	92538

5.4 BOUNDARY CONDITIONS

Boundary conditions are the set of conditions specified for the behaviour of the solution to a set of differential equations at the boundary of its domain. Boundary conditions are important in determining the mathematical solutions to many physical problems. These conditions specify the flow and thermal variables on the boundaries of a physical model. They are, therefore, a critical component of simulation and it is important that they are specified appropriately.

It is important to check the quality of mesh, because parameter such as skewness affects the accuracy of the CFD simulation. Each element has of value of skewness between 0 and 1.

The skewness is classified in two ways, EquiAngle skew and EquiSize skew. The smaller value of equiAngle skew and equisize skew are more acceptable. It is also important to verify that all of the elements in mesh have positive area/volume otherwise the simulation in solver is not possible.

The conditions that are applied for numerical simulation of the centrifugal slurry pump simulations are given below

- Mass flow inlet: It is the inlet face at suction pipe entry.
- Wall: It is applied to Inlet passage faces, rotating faces of impeller and fixed faces of volute casing.
- Pressure outlet: It is applied on outlet face at delivery pipe entry.
- Fluid zone: It is applied suction pipe, impeller passages, volute casing, inlet passage and delivery pipe.
- Slurry is added in material list by giving soot conditions density and molar mass. For bottom ash density and molar mass is taken 2250 kg/m^3 and 36.281g/mol. In case of fly ash density is taken 1990$kg/m^3$and 28.12 g/mol.
- Bottom ash specified diameter is taken as 168 micron and for fly ash 54 micron.
- For erosion calculation Finnie model is applied at all domains. In Finnie model velocity power factor is taken 2.3 and reference velocity is taken 590 m/s in case of steels.
- Simulations done on 1150r p m, 1300 r p m and 1450 r p m and mass flow rate is taken 3, 10 and 15 m^3/s. Concentration is taken 10%, 20%, 30%, 40% and 50% for fly and bottom ash.

5.5 EFFECT OF ASH CONCENTRATION ON EROSION RATE ON IMPELLER BLADE

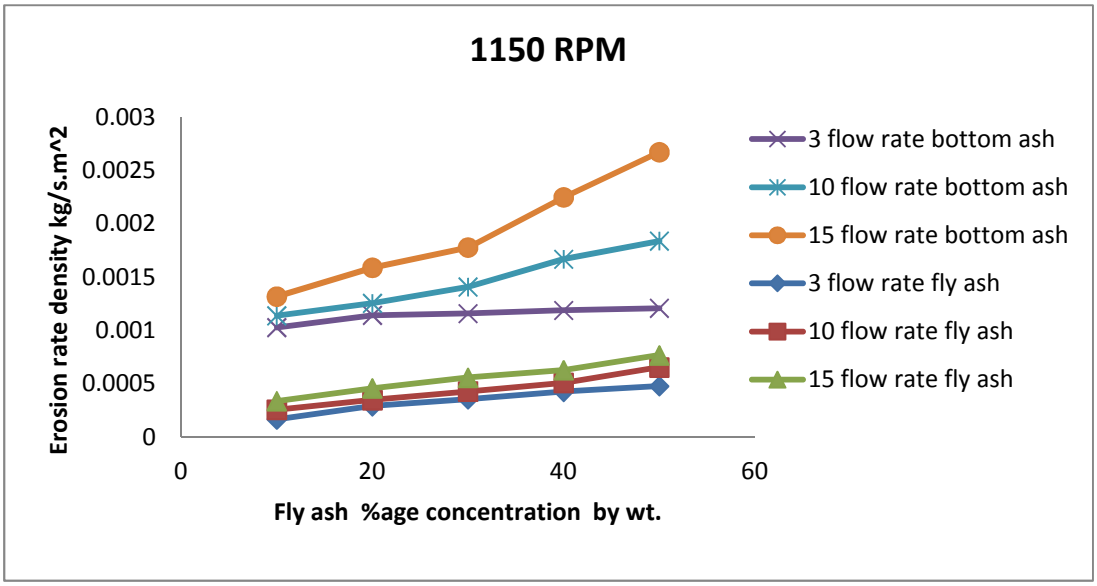

Figure 5.3 Erosion rate density vs concentration 1150 r p m

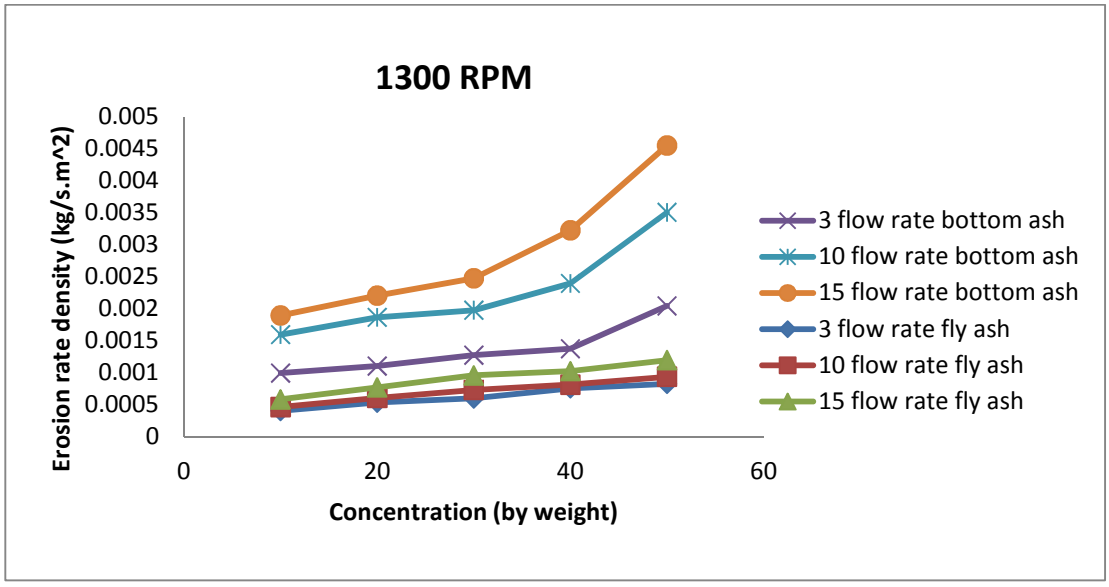

Figure 5.4 Erosion rate density vs concentration 1300 r p m

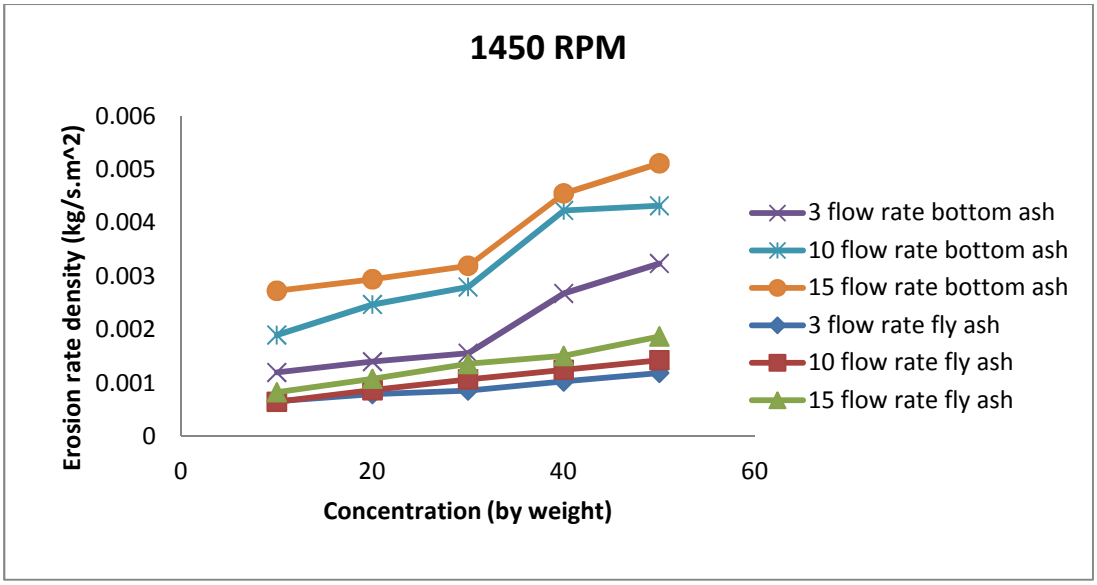

Figure 5.5 Erosion rate density vs concentration 1450 r p m

As the concentration of the particles in fluid increases, the effect of erosion rate on the blade is increases. However there is increase in erosion rate density on the blade. As shown in figure 5.3 to figure 5.5 the erosion rate is increases with the increase in concentration of ash and mass flow rate. It shows that more particles strikes on the blade and cause more erosion of the blades.

At 1150 r p m at all concentrations and mass flow rate erosion rate increases linearly. At

15 m^3/s flow rate by bottom ash it shows maximum erosion rate. At 1300 r p m erosion rate at mass flow rate 3m^3/s and 10 m^3/s shows less erosion rate increases but at 15 m^3/s sudden increases in erosion wear in linear passion. At 1450 r p m figure 5.5 shows more erosion takes place 15 m^3/s mass flow rate. With fly ash it shows 60% less erosion of the blades as compare to the bottom ash. Fly ash particles has less mean diameter as compare to the bottom ash particles diameter.

5.6 EFFECT OF ASH CONCENTRATION ON EROSION RATE ON HUB

As the concentration of the particles in fluid increases, the effect of erosion rate on the blade is increases. However there is linear increase in erosion rate density on the blade. As shown in figure 5.6 - 5.8 the erosion rate is increases with the increase in concentration of ash and mass flow rate. It shows that more particles strike on hub and causemore erosion of the hub.

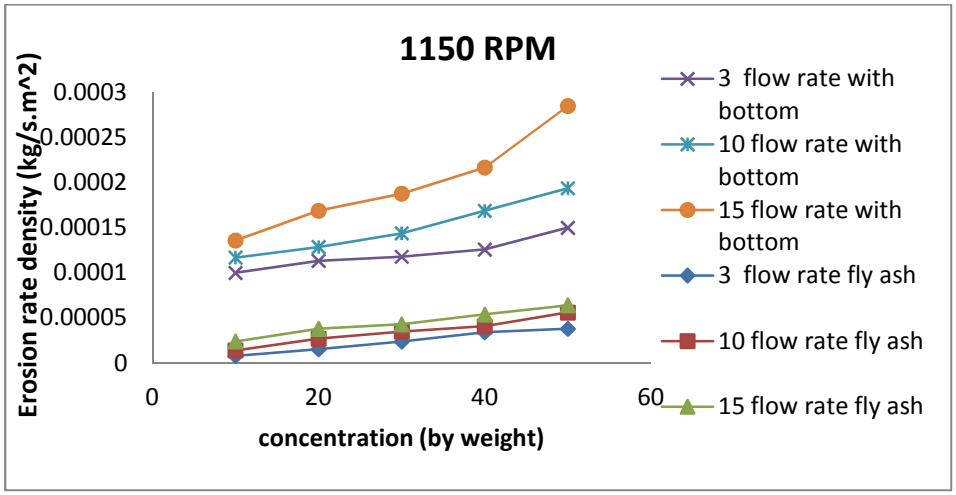

Figure 5.6 Erosion rate density vs concentration 1150 r p m

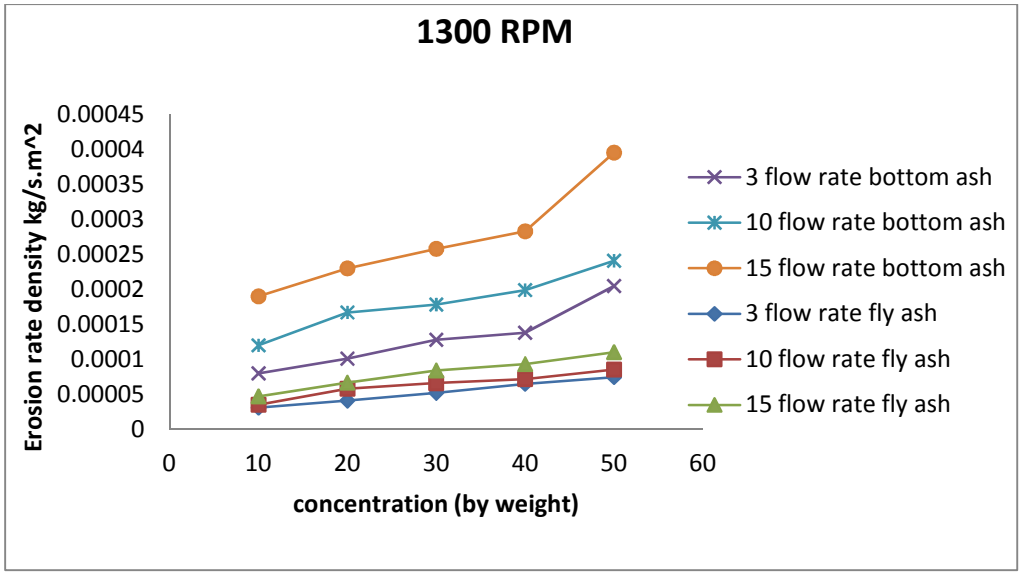

Figure 5.7 Erosion rate density vs concentration 1300 r p m

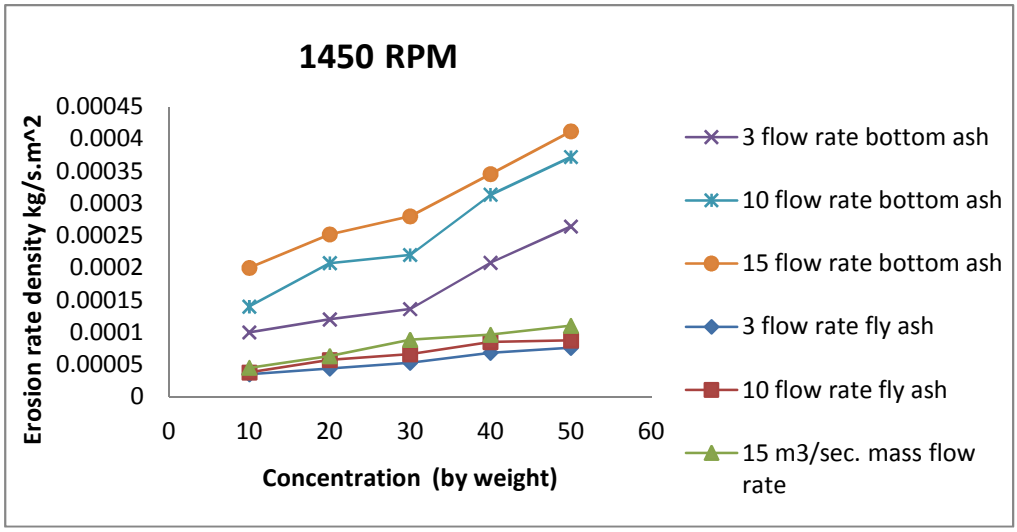

Figure 5.8 Erosion rate density vs concentration 1450 r p m

5.7 WEAR PATTERN ON THE BLADES OF IMPELLER BY BOTTOM ASH

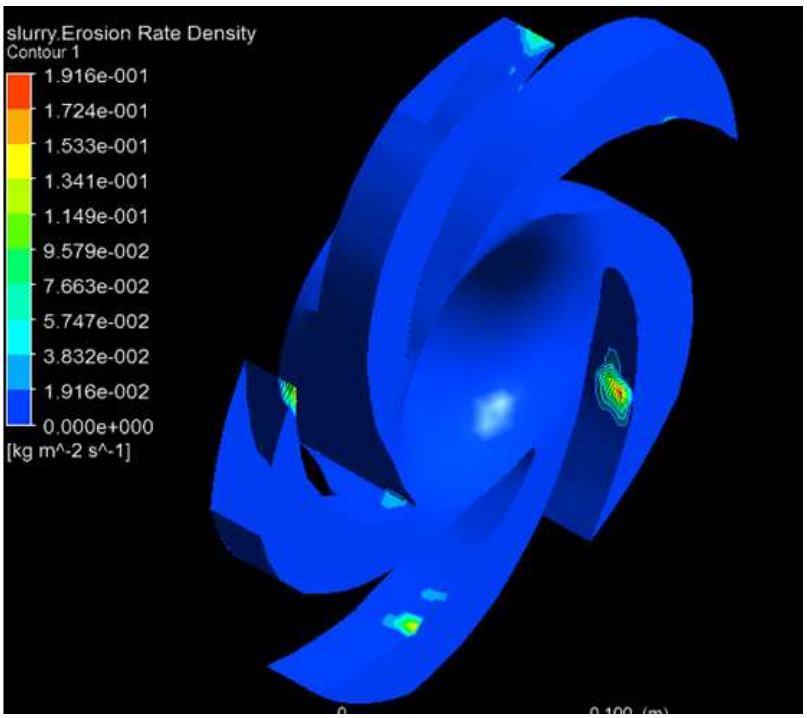

Figure 5.9 Erosion of the blade at 1450 r p m and 50% concentration bottom ash

As shown in figure 5.9 shows the erosion of the blade at 50% concentration at maximum speed 1450 r p m has maximum erosion. Red mark shows maximum erosion of the blade.

5.8 WEAR PATTERN OF IMPELLER BY FLY ASH

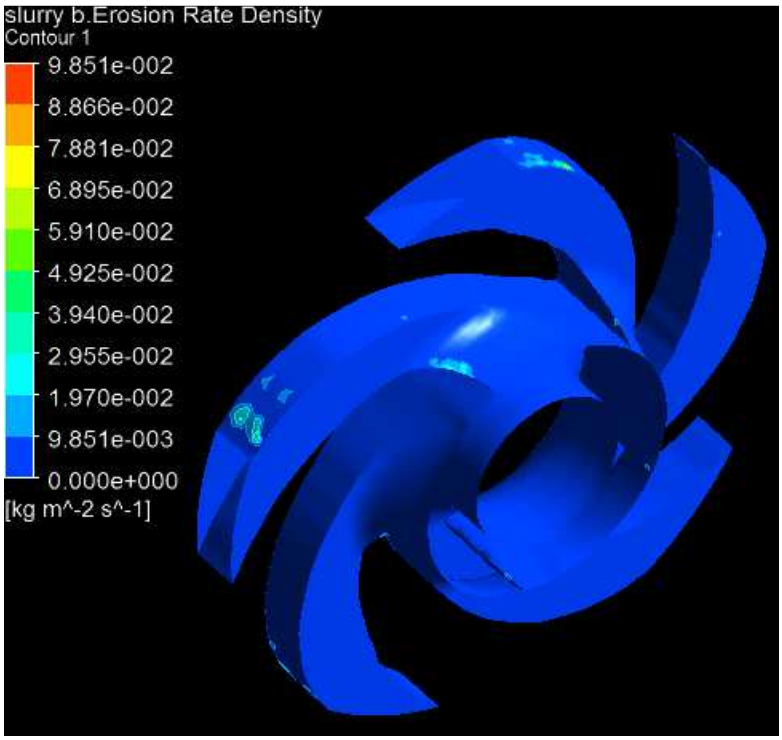

Figure 5.10 Erosion of the blade at 1450 r p m and 50% concentration fly ash

As shown in figure 5.10 shows the erosion of the blade at 50% concentration at maximum speed 1450 r p m has maximum erosion. Red mark shows maximum erosion of the blade. At the blade tip shows maximum erosion of the blade. Fly ash shows less erosion as compare to the bottom ash at the impeller.

CONCLUSION

- The results show that the erosion wear has strong dependence on flow rate. The higher the flow rate, the higher the wear rate of the test material. Solid concentration also affects the wear rate linearly.
- The effect of erosion rate is more on the blades than on the hub. The graph shows that the erosion rate density on the blades is nearly 8-10 times than on the hub.
- The effect of wear is more at leading edge than at trailing edge of blades. So selecting the optimized inlet blade angle can play a major role in reducing erosion wear and providing smooth flow for fluid.
- The electroplating technique is used for coating of chromium hard as a base material. From the experiment it is observed that erosion pot tester TR-41 used for the evaluation of the erosion wear of material in terms of loss of material by weight. From the experiment evaluation it is observed that erosion wear of pump material is a function of time, operation speed and concentration of the bottom and fly ash slurry. It is also reveals that with coating (chromium hard) on the pump materials rate of erosion wear decreases rapidly. Chromium coated steel shows approximately 1.5 times better performance than uncoated steel. Similarly chromium coated steel 316 shows approximately 2.5 times better performance than uncoated steel 316.

FUTURE SCOPE

The use of pumps for slurry transfer has increased by several folds. The scope of future work in this topic is very vast. A lot of work can be done in this field. Better designs and improved materials can increase the life of pumps to several more hundred hours.

1) The other affecting design parameters such as inlet blade angle, outlet blade angle, and the number of blades can be changed to see the effect of erosion rate and a optimized design could be developed which will have minimum erosion on the impeller.

2) Pump performance characteristics as well as velocity and pressure distribution can be studied.

3) Different types of materials can be tested for manufacturing of impeller and erosion patterns can be studied.

4) The present work of homogeneous flow can be extended to heterogeneous flows so that the effect of erosion behaviour can be evaluated for heterogeneous slurries.

5) Effect of cavitation on pump performance can be studied.

REFERANCES

1. Ping Li, QizhouCai, Bokang Wei (2005) "Failure analysis of the impeller of slurry pump used in zinc hydrometallurgy process", Engineering Failure Analysis, 13: 876–885
2. A. Hamed and W. Tabakoff (2006) "Erosion and Deposition in Turbomachinery", Journal of Propulsion and Power, 22:350-359
3. S. Ariely, A. Khentov (2006) "Erosion corrosion of pump impeller of cyclic cooling water system",Engineering Failure Analysis, 13: 925–932
4. J.F. Santa, J.C. Baena, A. Toro (2007) "Slurry erosion of thermal spray coatings and stainless steels for hydraulic machinery",Wear, 263: 258–264
5. J.F. Santa, L.A. Espitia et al (2009) "Slurry and cavitation erosion resistance of thermal spray coatings", Wear, 267: 160–167
6. ZhenlinLua, ZhiguoXingb, HuiXieC and Yongxin Zhou (2010) "Effect of SiC Particle Sizes on Erosion Wear Behaviour of SiC/Epoxy Resin Composite", Materials Science Forum, 658:368-371
7. Y. Wang, Y.G. Zheng, W. Kea, W.H. Sun, W.L. Hou, X.C. Chang, J.Q. Wang "Slurry erosion–corrosion behaviour of high-velocity oxy-fuel (HVOF) sprayed Fe-based amorphous metallic coatings for marine pump in sand-containing NaCl solutions", Corrosion Science, 53:3177–3185
8. Yan Liu,Lijun Wang, Hui Chen, MingjingTu (2012) "Influence of Sand variety on Erosion Wear Properties of Nanostructured WC-12Co coatings Deposited by HVOF Spraying",Advanced Materials Research , 396-398 :472-477
9. Hawthorne H.M. (2002) "Some Coriolis slurry erosion test developments", *Tribology International*, 35: 625–630
10. Weidong Zhou, Zhimei Zhao, T. S. Lee, and S. H.Winoto (2003) "Investigation of Flow Through Centrifugal Pump Impellers Using Computational Fluid Dynamics", *International Journal of Rotating Machinery*, 9(1): 49–61
11. R.J.K. Wood, T.F. Jones, J. Ganeshalingam, N.J. Miles. (2004) "Comparison of predicted and experimental erosion estimates in slurry ducts", *Wear*. 256:937–947

12. H.M. Badr, M.A. Habib, R. Ben-Mansour, S.A.M. Said. (2005) "Numerical investigation of erosion threshold velocity in a pipe with sudden contraction", *Computers & Fluids* .34:721–742

13. Miguel Asuaje, FaridBakir, SmineKouidri, Frank Kenyery, Robert Rey (2005) "Numerical Modelization of the Flow in Centrifugal Pump: Volute Influence in Velocity and Pressure Fields" , *International Journal of Rotating Machinery* ,3: 244–255

14. Gary Brown (2006) "Use of CFD to predict and reduce erosion in an industrial slurry piping system", Fifth International Conference on CFD in the Process Industries CSIRO, Melbourne, Australia

15. Subhash N. Shah, Samyak Jain (2007). "Coiled tubing erosion during hydraulic fracturing slurry flow", *Wear*. 264: 279–290

16. Khin Cho Thin, MyaMyaKhaing, and KhinMaung Aye, (2008), "Design and Performance Analysis of Centrifugal Pump",*World Academy of Science, Engineering and Technology*, 46: 422-429.

17. M. Sahu, Kishanjit Kumar Khatuaand KanhuCharanPatra, T. Naik. (2009), "Developed laminar flow in pipe using computational fluid dynamics" 7th International R&D Conference to be held in Bhubaneswar (India) from 4-6 February 2009.

18. L.J.W. Graham, D. Lester and J. Wu, (2009). "Slurry erosion in complex flows: Experimental and CFD" , Seventh International Conference on CFD in the Minerals and Process Industries , CSIRO, Melbourne, Australia ,9-11 December 2009.

19. Min-Hua Wang, Cunkui Huang, K. Nanda kumar, P. Minev, J. Luo and S. Chiovelli (2009) "Computational fluid dynamics modelling and experimental study of erosion in slurry jet flows" , *International Journal of Computational Fluid Dynamics*, 23:155–172

20. A Mittal, B K Gandhi, and KM Singh (2009) "Improvement in the design of a centrifugal impeller for an oil cooling blower system using computational fluid dynamics" , *Power and Energy*, 223: 981 -989.

21. R. Spence, J. Amaral-Teixeira (2009) "A CFD parametric study of geometrical variations on the pressure pulsations and performance characteristics of a centrifugal pump", *Computers & Fluids*, 38: 1243–1257

22. Dong Xing, Zhang Hai-lu, Wang Xin-yong (2009) "Finite element analysis of wear for centrifugal slurry pump", Procedia Earth and Planetary Science, 1:1532–1538

23. Yuh Ming Ferng, Bin Hong Lin, (2010), "Predicting the wall thinning engendered by erosion–corrosion using CFD methodology", *Nuclear Engineering and Design.* 240:2836–2841

24. SowjanyaVijiapurapu, Jie Cui. (2010) "Performance of turbulence models for flows through rough pipes", *Applied Mathematical Modelling.* 34 : 1458–1466

25. Maitelli, C. W. S. de P. , Bezerra, V. M. de F. , da Mata (2010) " simulation of flow in a centrifugal pump of esp systems using computational fluid dynamics", brazilian journal of petroleum and gas , 4:001-009

26. TAN Minggao, YUAN Shouqi, LIU Houlin, WANG Yong, and WANG Kai, (2010), "Numerical Research on Performance Prediction for Centrifugal Pumps", *Chinese Journal of mechanical engineering*, 23:1-8

27. Suanne Kruger, Nicolas Martin and Philippe Dupont (2010) "Assessment of wear erosion in pump impeller", Proceeding of the Twenty- Sixth International Pump Users Symposium, 51-56

28. Yuanqiang Tan, Hao Zhang, Dongmin Yang, Shengqiang Jiang, Junhua Song, Yong Sheng,(2011). "Numerical simulation of concrete pumping process and investigation of wear mechanism of the piping wall", *Tribology International*. 46:137-144.

29. Z.A. Majid, R. Mohsin, M.Z. Yusof (2011) "Experimental and computational failure analysis of natural gas pipe", *Engineering Failure Analysis*. 19 : 32–42

30. Xue-Guan Song, Joon-Hong Park, Seung-Gyu Kim, Young-Chul Park (2011) "Performance comparison and erosion prediction of jet pumps by using a numerical method" , *Mathematical and Computer Modeling*, 10:1-6

31. REN Neifei, CHEN Mingmin, JIANG Jie and CHENG Li (2011) "Flow Numerical Simulation of Centrifugal Pump with Splitting Blades based on Reverse Engineering", Applied Mechanics and Materials, 43: 691-694

32. Shaoping Zhou, PeiwenLv, Xiaoxia Ding**,** Yongsheng Su and Dequan Chen (2012) "Numerical Simulation and Impeller Optimization of a Centrifugal Pump", Advanced Materials Research, 472-475:2195-2198

33. Qiang Zhang, Qiu-shuangSong,Jun Mao (2011) "Numerical Simulation of Erosion and Particle Motion of Multi- Medium Oil -Coal-Water Slurry Pump", Advanced Materials Research, 346 :398-404

34. Chong Y. Wonga, Christopher Solnordal, Anthony Swallow, Steven Wang, Lachlan Graham, Jie Wu (2012) "Predicting the material loss around a hole due to sand erosion", Wear, 276– 277:1– 15

APPENDIX

Weight loss (gm) / Time (min.)	At 20% C_w by wt.		At 40% C_w by wt.		At 60% C_w by wt.	
	Bottom ash	Fly ash	Bottom ash	Fly ash	Bottom ash	Fly ash
60	0.018	0.0027	0.024	0.004	0.0461	0.0078
90	0.0207	0.0035	0.0281	0.0053	0.0581	0.0085
150	0.024	0.0041	0.0387	0.0065	0.0673	0.0089
120	0.0374	0.0054	0.0408	0.0073	0.0836	0.0096

Table 1.Variation of weight loss v/s time of steel 316 at 700r p m speed

Weight loss (gm) / Time (min.)	At 20% C_w by wt.		At 40% C_w by wt.		At 60% C_w by wt.	
	Bottom ash	Fly ash	Bottom ash	Fly ash	Bottom ash	Fly ash
60	0.0158	0.0053	0.021	0.0062	0.0313	0.0192
90	0.0228	0.0065	0.032	0.01	0.0497	0.0208
150	0.0344	0.0079	0.0437	0.0127	0.0643	0.0222
120	0.0452	0.0088	0.0572	0.0187	0.0818	0.00976

Table 2.Variation of weight loss v/s time of steel 316 at 1000r p m speed

Weight loss (gm) / Time (min.)	At 20% C_w by wt.		At 40% C_w by wt.		At 60% C_w by wt.	
	Bottom ash	Fly ash	Bottom ash	Fly ash	Bottom ash	Fly ash
60	0.0343	0.0125	0.0474	0.0212	0.0613	0.0416
90	0.0404	0.0184	0.0584	0.0279	0.0855	0.0452
150	0.0511	0.0251	0.0756	0.0350	0.103	0.0491
120	0.0646	0.0157	0.0944	0.0388	0.138	0.0523

Table 3.Variation of weight loss v/s time of steel 316 at 1400r p m speed

Weight loss (gm) / Time (min.)	At 20% C_w by wt. Bottom ash		At 40% C_w by wt. Bottom ash		At 60% C_w by wt. Bottom ash	
	Uncoated	Coated	Uncoated	Coated	Uncoated	Coated
60	0.018	0.0077	0.024	0.0116	0.0461	0.0155
90	0.0207	0.0087	0.0281	0.01308	0.0581	0.0171
150	0.024	0.0104	0.0387	0.0157	0.0673	0.0198
120	0.0374	0.0121	0.0408	0.0162	0.0836	0.0219

Table 4.Variation of weight loss v/s time of coated and uncoated steel 316 at 700r p m speed

Weight loss (gm) / Time (min.)	At 20% C_w by wt. Bottom ash		At 40% C_w by wt. Bottom ash		At 60% C_w by wt. Bottom ash	
	Uncoated	Coated	Uncoated	Coated	Uncoated	Coated
60	0.0158	0.0176	0.021	0.0248	0.0313	0.0424
90	0.0228	0.0191	0.032	0.0263	0.0497	0.0512
150	0.0344	0.0223	0.0437	0.0282	0.0643	0.0621
120	0.0452	0.0245	0.0572	0.0306	0.0818	0.0708

Table 5.Variation of weight loss v/s time of coated and uncoated steel 304 at 1000r p m speed

Weight loss (gm) / Time (min.)	At 20% C_w by wt. Bottom ash		At 40% C_w by wt. Bottom ash		At 60% C_w by wt. Bottom ash	
	Uncoated	Coated	Uncoated	Coated	Uncoated	Coated
60	0.0343	0.0414	0.0474	0.0598	0.0613 0.0795	
90	0.0404	0.0456	0.0584	0.0731	0.0855	0.1146
150	0.0511	0.0516	0.0756	0.0895	0.103	0.1563
120	0.0646	0.0570	0.0944	0.1026	0.138	0.1931

Table 6.Variation of weight loss v/s time of coated and uncoated steel 304 at 1400r p m speed

Weight loss (gm) / Time (min.)	At 20% C_w by wt.		At 40% C_w by wt.		At 60% C_w by wt.	
	Bottom ash	Fly ash	Bottom ash	Fly ash	Bottom ash	Fly ash
60	0.011	0.0035	0.0132	0.0038	0.0192	0.0045
90	0.0129	0.0041	0.0152	0.0046	0.0214	0.0054
150	0.0132	0.0045	0.0171	0.0051	0.0245	0.0061
120	0.0155	0.0052	0.01944	0.0058	0.0277	0.0080

Table 7.Variation of weight loss v/s time of steel 420 at 700r p m speed

Weight loss (gm) / Time (min.)	At 20% C_w by wt.		At 40% C_w by wt.		At 60% C_w by wt.	
	Bottom ash	Fly ash	Bottom ash	Fly ash	Bottom ash	Fly ash
60	0.0116	0.0041	0.0202	0.0053	0.0562	0.0108
90	0.0163	0.0050	0.0257	0.0065	0.0629	0.0124
150	0.0217	0.0065	0.0318	0.0081	0.0698	0.0146
120	0.0274	0.0080	0.0491	0.0098	0.0237	0.0174

Table 8.Variation of weight loss v/s time of steel 420 at 1000r p m speed

Weight loss (gm) / Time (min.)	At 20% C_w by wt.		At 40% C_w by wt.		At 60% C_w by wt.	
	Bottom ash	Fly ash	Bottom ash	Fly ash	Bottom ash	Fly ash
60	0.032	0.0058	0.047	0.0114	0.099	0.0287
90	0.049	0.0081	0.0672	0.0135	0.1322	0.0325
150	0.0672	0.0118	0.0808	0.0158	0.175	0.0389
120	0.0719	0.0156	0.0992	0.0196	0.2149	0.0457

Table 9.Variation of weight loss v/s time of steel 420 at 1400rpm speed

Weight loss (gm) / Time (min.)	At 20% C_w by wt. Bottom ash		At 40% C_w by wt. Bottom ash		At 60% C_w by wt. Bottom ash	
	Uncoated	Coated	Uncoated	Coated	Uncoated	Coated
60	0.011	0.0009	0.0132	0.0117	0.0192	0.0157
90	0.0129	0.0082	0.0152	0.0128	0.0214	0.0185
150	0.0132	0.0106	0.0171	0.0136	0.0245	0.0213
120	0.0155	0.0122	0.0194	0.0169	0.0277	0.0239

Table 10.Variation of weight loss v/s time of coated and uncoated steel 420 at 700rpm speed

Weight loss (gm) / Time (min.)	At 20% C_w by wt. Bottom ash		At 40% C_w by wt. Bottom ash		At 60% C_w by wt. Bottom ash	
	Uncoated	Coated	Uncoated	Coated	Uncoated	Coated
60	0.0116	0.0106	0.0202	0.0192	0.0562	0.0523
90	0.0163	0.0112	0.0257	0.0217	0.0629	0.0548
150	0.0217	0.0187	0.0318	0.0276	0.0698	0.0637
120	0.0274	0.0210	0.0491	0.0437	0.0237	0.0189

Table 11.Variation of weight loss v/s time of coated and uncoated steel 420 at 1000 rpm speed

Weight loss (gm) / Time (min.)	At 20% C_w by wt. Bottom ash		At 40% C_w by wt. Bottom ash		At 60% C_w by wt. Bottom ash	
	Uncoated	Coated	Uncoated	Coated	Uncoated	Coated
60	0.032	0.028	0.047	0.039	0.099	0.081
90	0.049	0.037	0.0672	0.0579	0.1322	0.1278
150	0.0672	0.0582	0.0808	0.0728	0.175	0.167
120	0.0719	0.0673	0.0992	0.0957	0.2149	0.2098

Table 12.Variation of weight loss v/s time of coated and uncoated steel 420 at 1400 r p m speed